# FOXM1-Specific TCR-Engineered T Cells Target Non–Small Cell Lung Cancer

Emily Bontekoe[1], Minying Zhang[1], Peixin Jiang[1], Amanda Montoya[1], Yulia Shulga[2], Jared K. Slone[3], Emily Paul[4], Christopher Polera[4], Sarah Forward[2], Barbara Nassif Rausseo[1,5], Emane Rose Assita[2], Changsheng Xing[1], David P. Molkentine[1], Benjamin B. Morris[1], Isabella Polic[1], Janos Roszik[5], Ricardo Salgado[6], Aria Vaishnavi[1,7], Drew Deniger[1], Hai T. Tran[1], Don L. Gibbons[1], Ara Vaporciyan[8], Maura L. Gillison[1], Ignacio I. Wistuba[1,9], Lydia E. Kavraki[3], Jianjun Zhang[1,10], Gregory Lizee[5], Cassian Yee[5], Patrick Hwu[4], Sheldon Kwok[2], Alex M. Jaeger[4], John V. Heymach[1], and Alexandre Reuben[1]

## ABSTRACT

FOXM1 is highly expressed in various cancer types and considered a key driver of cancer progression. Accordingly, we evaluated the immunogenicity of FOXM1 and investigated the feasibility of targeting this transcription factor using T-cell receptor (TCR) engineering. We identified epitopes derived from FOXM1 which were immunogenic on HLA-A*02:01, HLA-A*24:02, and HLA-A*23:01, endogenously processed and presented, and resulted in T-cell activation and cytotoxic T-cell responses. Following the generation of TCR-T cells, sensitivity and specificity were confirmed by peptide dose–response and X-scan, respectively. Most importantly, adoptive transfer of TCR-engineered T cells led to a significant reduction in tumor growth, as well as significantly prolonged survival in a tumor-bearing immunocompromised murine model. Our studies confirm the immunogenicity of FOXM1 and feasibility of targeting this antigen using TCR engineering.

## Introduction

Lung cancer is the leading cause of cancer-related mortality globally among both men and women (1). Non–small cell lung cancer (NSCLC) remains the most common subtype of lung cancer, accounting for approximately 85% of all cases worldwide (2). Despite advances in early detection and therapeutic strategies, NSCLC continues to be associated with low overall survival (3). Although smoking prevalence has declined due to public health initiatives, the incidence of lung cancer remains high (4). Standard treatment paradigms for NSCLC typically involve a multimodal approach, including surgical resection for early-stage disease, adjuvant chemotherapy, and radiotherapy (5). For advanced stages, targeted therapies [tyrosine kinase inhibitors (TKI) and immune checkpoint inhibitors (ICI)] are now recognized as key therapeutic approaches. In solid malignancies associated with high tumor mutational and neoantigen burdens, ICIs such as anti–PD-1/PD-L1 and anti–CTLA-4 have provided broad T-cell reactivation and enhanced antitumor T-cell responses (6). Despite these advances in ICIs, up to 64% of patients with NSCLC develop acquired resistance when administered as a second-line treatment, whereas many fail to initially respond (7, 8). Similarly, TKIs have demonstrated the ability to prolong progression-free survival in advanced NSCLC; however, efficacy has plateaued as the development of resistance inevitably occurs (8–10). Overall, these therapies have demonstrated limited long-term efficacy, and consequently, identifying therapeutic strategies is critical in improving long-term survival in patients with NSCLC.

T-cell receptor (TCR) engineering of T cells (TCR-T cell) represents a promising cellular therapy approach. TCR-T cells can target tumor-associated antigens (TAA) or neoantigens presented by tumor cells on MHC/HLA molecules. Neoantigens arise from somatic mutations, resulting in the presentation of unique epitopes at the tumor cell surface (11). However, neoantigens tend to be highly personalized and patient-specific (11, 12). In contrast, TAAs provide broader applicability and may therefore streamline the therapeutic development process as they are shared across patient populations and tumor types, thereby benefitting a larger patient population (13, 14). TAAs may conversely result in on-target, off-tumor toxicity due to their occasional expression in normal tissues, highlighting the critical role of antigen selection and safety testing for TCR-T cells.

The transcription factor Forkhead box protein M1 (FOXM1) has been proposed as a TAA that plays a critical role in cell-cycle regulation (15). Importantly, FOXM1 contributes to tumorigenesis by promoting cell proliferation, survival, invasion, and angiogenesis (16). FOXM1 is highly expressed in various cancers, including breast, lung, pancreatic, and colorectal cancers, among many others.

[1]Department of Thoracic/Head & Neck Medical Oncology, The University of Texas MD Anderson Cancer Center, Houston, Texas. [2]LASE Innovation, Waltham, Massachusetts. [3]Department of Computer Science, Rice University, Houston, Texas. [4]Department of Molecular Oncology, H. Lee Moffitt Cancer Center and Research Institute, Tampa, Florida. [5]Department of Melanoma Medical Oncology, The University of Texas MD Anderson Cancer Center, Houston, Texas. [6]Salgado Family Charitable Fund, Miami, Florida. [7]Department of Genetics, The University of Texas MD Anderson Cancer Center, Houston, Texas. [8]Department of Thoracic and Cardiovascular Surgery, The University of Texas MD Anderson Cancer Center, Houston, Texas. [9]Department of Translational Molecular Pathology, The University of Texas MD Anderson Cancer Center, Houston, Texas. [10]Department of Genomic Medicine, The University of Texas MD Anderson Cancer Center, Houston, Texas.

E. Bontekoe and M. Zhang co-first authors.

**Corresponding Author:** Alexandre Reuben, Thoracic/Head & Neck Medical Oncology, The University of Texas MD Anderson Cancer Center, 1515 Holcombe Blvd, Houston, TX 77030. E-mail: areuben@mdanderson.org

Cancer Immunol Res 2026;14:958–73

**doi:** 10.1158/2326-6066.CIR-25-0605

In NSCLC, studies have demonstrated that the upregulation of FOXM1 is associated with epithelial–mesenchymal transition and metastatic progression (17, 18). High FOXM1 expression has also been associated with worse overall survival in adrenocortical carcinoma, glioma, colon adenocarcinoma, kidney carcinoma, liver carcinoma, lung adenocarcinoma, uterine carcinoma, and uveal melanoma, making it an attractive immunotherapeutic target (19). In this study, we identified and functionally characterized FOXM1-specific TCR-T cells isolated from blood of healthy donors and patients with lung cancer in order to demonstrate the potential of TCR-T cells targeting this prevalent antigen *in vitro* and *in vivo*.

## Materials and Methods

### Cell lines

Cell lines H1975 (RRID: CVCL_1511, 2023) and HEK-293 (RRID: CVCL_0045, 2020) were purchased from the ATCC. The H1975 cell line was cultured in complete medium, which included RPMI-1640 medium (Corning, 10040CV) supplemented with 10% FBS (GenDEPOT, F0601-050) and 1% penicillin–streptomycin (HyClone, SV30010). The HEK-293 cell line, which was cultured with DMEM (Corning, 100213CV) supplemented with 10% FBS (GenDEPOT, F0601-050) and 1% penicillin–streptomycin (HyClone, SV30010). DFCI032 (RRID: CVCL_A763), was established at Dana-Farber Cancer Institute, obtained in 2011, and cultured in complete medium. The patient-derived MDA-L-30 cell line was generated in 2021 and cultured in complete medium. H1975, HEK-293, DFCI032, and MDA-L-30 cell lines were passaged <5 times using trypsin EDTA (Gibco, 25200056) to detach cells and spun at 350 g for 5 minutes at room temperature. All cell lines were authenticated by MD Anderson Cancer Center Cytogenetics and Cell Authentication Core by short tandem repeat DNA profiling and tested negative for *Mycoplasma* contamination (Lonza, LT07-218). Target tumor cells (H1975 and HEK-293) were transduced with HLA alleles A*02:01 (VectorBuilder, VB190122-1151ffw), A*24:02 (VectorBuilder, VB190305-1184gac), and A*23:01 (Twist Bioscience), as well as FOXM1 genes. HLA-A*23:01 and FOXM1 genes were cloned with pENTER vector by GenScript USA, Inc. (RRID: SCR_002891). Final HLA-A*23:01 allele constructs were created by Gateway LR Clonase II Enzyme Mix (Invitrogen, 11791020) into a lentiviral vector, pLV401GFP (GenScript, RRID: SCR_002891; ref. 20). Tumor cells successfully transduced with HLAs were sorted by GFP expression. FOXM1 was cloned into PHAGE vector (Addgene, 24526), isolated by puromycin selection, and overexpressed in tumor cell lines expressing desired HLA. Primary cell lines, including those arising from the heart (AC16; ATCC, CRL-3568), lung (HBEC3-KT; graciously provided by Dr. Yongxing Wang's laboratory at MD Anderson Cancer Center), liver (HC3716-hTert; graciously provided by Dr. Lawrence Kwong's laboratory at MD Anderson Cancer Center), kidney (HEK-293; ATCC, CRL-1573), and brain (AST-1, graciously provided by Dr. Jian Hu's laboratory at MD Anderson Cancer Center). The AC16 cell line was cultured in DMEM:F12 medium (ATCC, 30-2006) supplemented with 12.5% FBS (GenDEPOT, F0601-050) and centrifuged at 125 g for 7 minutes at room temperature. The HBEC3-KT cell line was cultured in Airway Epithelial Cell Basal Medium (ATCC, PCS-300-030) supplemented using Bronchial Epithelial Cell Growth Kit (ATCC, PCS-300-040) and centrifuged at 210 g for 5 minutes at room temperature. The HC3716-hTert cell line was cultured in HCM Basal Medium (Lonza, CC-3199) and HCM SingleQuot Supplements (CC-4182) supplemented with 5% FBS (GenDEPOT, F0601-050) and 10% human serum (GeminiBio, 100-512) and centrifuged at 100 g for 8 minutes at room temperature. The HEK-293 cell line was cultured with DMEM (Corning, 100213CV) supplemented with 10% FBS (GenDEPOT, F0601-050) and 1% penicillin–streptomycin (HyClone, SV30010). The AST-1 cell line was cultured in DMEM (Corning, 100213CV) supplemented with 10% FBS (GenDEPOT, F0601-050), 1% penicillin–streptomycin (HyClone, SV30010), and 2 mmol/L L-Glutamine (Cytiva, SH3003401) and centrifuged at 150 g for 10 minutes. All were obtained in 2025, tested negative for *Mycoplasma* contamination (Lonza, LT07-218), passaged <5 times using trypsin EDTA (Gibco, 25200056) to detach cells, and transduced with HLA-A*02:01 by lentiviral vector pLV401 (VectorBuilder, VB190102-1131btg). Positive HLA-A*02:01 cells were sorted by flow cytometry at the North Campus MD Anderson Cancer Center Flow Cytometry Core.

### Protein expression

FOXM1 expression was evaluated by Western blot in essential primary cell lines (AC16, AST-1, HC3716-hTert, HEK-293, and HBEC3-KT) and the tumor cell line, H1975, using a monoclonal FOXM1 (D12D5) primary antibody (Cell Signaling Technology, 5436S) and Amersham ECL rabbit IgG secondary antibody (Cytiva, NA934). Protein lysates were separated on Criterion TGX Stain-Free Precast Gels (Bio-Rad, 4561094) and transferred onto polyvinylidene difluoride membranes using the Trans-Blot Turbo Transfer System (Bio-Rad, 1704157). Membranes were probed with FOXM1 and normalized to β-actin (Cell Signaling Technology, 8457T) following standard protocols. Proteins were detected using enhanced chemiluminescence reagents (Supersignal West Femto Maximum Sensitivity Substrate, Thermo Fisher Scientific, 34096) and visualized with chemiluminescence detection system (ChemiDoc Imaging System, Bio-Rad).

### Patient cohort and datasets

FOXM1 RNA expression of publicly available lung cancer patient data ($n$ = 1,018) was obtained from The Cancer Genome Atlas (TCGA) and compared with normal tissue transcript expression from GTEx (21, 22). Normal tissue expression analysis included muscle–skeletal ($n$ = 564), brain–cerebellar hemisphere ($n$ = 136), brain–hypothalamus ($n$ = 121), brain–hippocampus ($n$ = 123), heart–left ventricle ($n$ = 303), brain–putamen ($n$ = 124), heart–atrial appendage ($n$ = 297), brain–cerebellum ($n$ = 173), brain–amygdala ($n$ = 100), brain–substantia nigra ($n$ = 88), artery–tibial ($n$ = 441), pancreas ($n$ = 248), brain–caudate ($n$ = 160), brain–frontal cortex ($n$ = 129), brain–anterior cingulate cortex ($n$ = 121), brain–cortex ($n$ = 158), brain–nucleus accumbens ($n$ = 147), brain–spinal cord ($n$ = 91), esophagus–muscularis ($n$ = 370), esophagus–gastroesophageal junction ($n$ = 244), colon–sigmoid ($n$ = 233), pituitary ($n$ = 183), uterus ($n$ = 111), artery–aorta ($n$ = 299), nerve–tibial ($n$ = 414), cervix–endocervix ($n$ = 5), adipose–visceral (omentum; $n$ = 355), liver ($n$ = 175), artery–coronary ($n$ = 173), breast–mammary tissue ($n$ = 290), fallopian tube ($n$ = 7), kidney–cortex ($n$ = 45), ovary ($n$ = 133), bladder ($n$ = 11), adrenal gland ($n$ = 190), thyroid ($n$ = 446), whole blood ($n$ = 407), prostate ($n$ = 152), adipose (subcutaneous; $n$ = 11,215), minor salivary gland ($n$ = 97), stomach ($n$ = 262), lung ($n$ = 427), cervix–ectocervix ($n$ = 6), skin–not sun-exposed ($n$ = 387), skin–sun-exposed ($n$ = 473), vagina ($n$ = 115), colon–transverse ($n$ = 274), small intestine–terminal ileum ($n$ = 137), spleen ($n$ = 162), esophagus–mucosa ($n$ = 407), and testis ($n$ = 259). Data were analyzed by GraphPad Prism (GraphPad). Available data from two independent

cohorts (ICON cohort, $n = 104$; and PROSPECT cohort, $n = 275$) of localized and resected NSCLC at the University of Texas MD Anderson Cancer Center were assessed for FOXM1 expression displayed at transcripts per million (TPM) and TCR sequences using available RNA sequencing (RNA-seq), RNA microarray data, and bulk TCR repertoire sequencing (23, 24). Both ICON (PA15-111) and PROSPECT (LAB07-0233) protocols were approved by the Institutional Review Board (IRB) of University of Texas MD Anderson Cancer Center, complying with all federal, state, and local regulatory guidelines, and in alignment with Good Clinical Practice Guidelines and the Declaration of Helsinki. All subjects enrolled in these research studies provided signed informed consent prior to protocol enrollment. The analysis of ICON and PROSPECT cohorts was independent of sex, age, randomization, or group size of subjects. FOXM1 protein expression data in normal tissues were obtained from the Human Protein Atlas (UniProt: Q08050), in which samples were analyzed by conventional immunohistochemistry and classified as not detected, low, medium, and high based on knowledge-based annotations (Human Protein Atlas, proteinatlas.org). FOXM1 protein expression was correlated with mRNA expression using publicly available NSCLC data (cBioPortal.org).

### TAA peptide prediction

Potential FOXM1 epitopes were identified using NetMHCpan4.1 (25). Epitope candidates were selected based on their predicted ability to strongly bind (% rank <0.5) to the top 10 most prevalent HLA class I alleles in the United States (14). Peptides were synthesized by Genemed Synthesis, Inc. and GenScript USA, Inc. with a purity >95%.

### Immunopeptidomics sample preparation

Nine NSCLC cell lines (A549, Calu6, HCC15, H1792, H1975, H2122, H460, HCC1171, and HCC78) were treated with 20 ng/mL of IFNγ for 48 hours and screened for FOXM1 epitopes by mass spectrometry. Immunopeptidomes of target cell lines, including H1975, H1975 (HLA-A*02:01), and H1975 FOXM1 (HLA-A*02:01), were further analyzed by liquid chromatography–tandem mass spectrometry (LC-MS/MS) following treatment with IFNγ or under untreated conditions. LC-MS/MS methods were adapted and modified from previously published methodologies to suit specific requirements for this study (26). W6/32 conjugation to Protein-A Sepharose 4B beads was carried out as previously described (26). To extract HLA I peptides from cell lines, 50 to 100 million cells were lysed with 1.75 mL fresh MHC-I extraction buffer [(MEB, 20 mmol/L Tris pH 8 (Invitrogen, AM9856)], 1 mmol/L EDTA (Thermo Fisher Scientific, 15575020), 100 mmol/L sodium chloride (Sigma-Aldrich, S3014), 1% Triton X 100 (Sigma-AldrichX100), 60 mmol/L octyl β-D-glucopyranoside (Sigma-Aldrich, O8001), 6 mmol/L magnesium chloride (Sigma-Aldrich, M8266), 39.1 mL nuclease-free $H_2O$ (Thermo Fisher Scientific, 43-879-36) + 0.2 mmol/L iodoacetamide (Thermo Fisher Scientific, A39271), and 1X HALT protease inhibitor (Thermo Fisher Scientific, 78429). Benzonase nuclease (1:1,000, Sigma-Aldrich, E1014-25KU) was added, and the lysate was rotated for 30 minutes at 4°C. During the lysate rotation, beads were equilibrated by transferring HLA-I antibody (W6/32)-conjugated bead slurry (100 μL/sample) to a new tube and adding MEB without HALT and iodoacetamide and then spun for 2 minutes (100 rcf at 4°C). The beads were washed again with MEB and spun down before being resuspended to create a 50% bead slurry. After lysate rotation, cell debris was pelleted (14,000 rcf for 15 minutes at 4°C), and the cleared supernatant was transferred to a new tube. Input (50 μL) was taken and stored for future Western blots. Prepared beads (100 μL) were added to each sample and rotated for 3 hours (4°C). After rotation, the beads were spun down at 100 rcf at 4°C, and the supernatant was collected as flow through. The beads were washed twice in MEB, twice in 1× PBS (Alkali Scientific, PB500), and twice in 10 mmol/L Tris pH 8. On the last wash, bead slurry was transferred to a clean low-binding microcentrifuge tube. MHC-bound peptides were then eluted with aqueous 1% trifluoroacetic acid (TFA) and incubated for 10 minutes at room temperature and intermittently flicked to keep the beads resuspended. During incubation, the following sets of solvents were made: buffer A (80% ACN + 0.1% FA) and buffer B (0.1% FA + $H_2O$; FA, Honeywell, 14281), wash buffer (3% ACN + 0.1% FA), and elution buffer (50% ACN + 0.1% FA). After TFA incubation, the beads were pelleted for 5 minutes 10,000 rcf at 4°C. Eluted peptides were then desalted on C18 Affinisep Spin tips (Thermo Fisher Scientific, NC3672893). Tips were prepped by washing the C-18 resin with ACN (50 μL), buffer A, and then buffer B with a spin (700 rcf for 1 minute) following each wash. After bead precipitation, 5 μL was taken for Western blotting, and the remaining supernatant was transferred into the Affinisep tip and spun for 3 minutes at 700 rcf. The Affinisep tip was then washed with wash buffer and spun (3 minutes at 700 rcf). Peptides were then eluted directly into the autosampler with two spins of 15 μL elution buffer. Peptides were dried down in a speed vac, and then peptides were reconstituted in 2% ACN, 0.1 μmol/L PRTC (Thermo Fisher Scientific, 88321), and 0.1% FA prior to mass spectrometry analysis.

For LC-MS/MS, HLA peptides were analyzed using a Thermo Orbitrap Ascend Tribrid mass spectrometer (Thermo Fisher Scientific) coupled with a Vanquish Neo UHPLC system (Thermo Fisher Scientific), equipped with a FAIMS Pro Duo interface. Samples were resuspended in 2% ACN + 0.1% FA and directly loaded onto a precolumn (2 cm × μm ID packed with C18 reversed-phase resin, 5 μm, 100 Å) in solvent A (2% ACN and 0.1% FA). Trapped peptides were eluted onto the analytic capillary chromatography column with an integrated electrospray tip (C18, 75 μm ID × 25 cm, 2 μm, 100 Å, Thermo Fisher Scientific). Peptides were eluted over 105 minutes with the following: gradient 2% to 3% solvent B (90% ACN and 0.1% FA) for 10 minutes, 3% to 5% solvent B for 2 minutes, 5% to 23% solvent B for 63 minutes, 23% to 40% solvent B for 22 minutes, 40% to 90% solvent B for 3 minutes, and hold for 5 minutes, followed by column equilibration and wash. Data-dependent acquisition (DDA) was performed in positive ion mode at a spray voltage of 2.0 kV and heated capillary temperature, 275°C. Full-scan mass spectra (300–1,000 m/z, 120,00 resolution) were detected in the Orbitrap analyzer after accumulation of $2.5 \times 10^6$ ions (normalized automatic gain control target of 250%) and 250 milliseconds maximum injection time. For every full scan, $MS^2$ spectra were collected during a 1.5-second cycle time for FAIMS compensation voltages at −45 and −65. Precursor ions were isolated with a 2.0 m/z isolation window, and accumulation time was set to auto. Ions were fragmented with higher energy disassociation collision with 30% collision energy at a resolution of 30,000. Charge states <2 and >4 were excluded, and dynamic exclusion was set to 15 seconds after $n = 1$ observation.

Immunopeptidomics database search by DDA in mass spectrometry was performed with FragPipe using the HLA workflow against a custom database containing the Gencode v42 human proteome supplemented with smORFs and the nuORF db v1.0. Group-specific FDR was set to 1%. The search was completed with nonspecific protein digestion, methionine oxidation, cysteine

carbamidomethylation, and protein N-term acetylation as variable modifications and peptide length 8 to 11 amino acids. Search outputs were subsequently analyzed and visualized in R or Skyline. Manual spectrum inspection was performed in PDV v2.2.

### Stimulation of antigen-specific T cells

Healthy donor leukaphereses were purchased from Charles River Laboratories, and all cells were processed for peripheral blood mononuclear cell (PBMC) isolation by Ficoll gradient centrifugation (RRID: SCR_003792). PBMCs from a single patient were collected at MD Anderson Cancer Center apheresis clinic by standard pheresis protocol in accordance to standard pheresis eligibility, processed under Good Manufacturing Practices conditions, and cryopreserved in liquid nitrogen. Collection was approved by the IRB of the University of Texas MD Anderson Cancer Center, complying with all federal, state, and local regulatory guidelines, and in alignment with all ethical standards. The patients enrolled provided signed informed consent prior to protocol enrollment. Monocytes from normal donor PBMCs were cultured for 1 week in AIM-V medium (Gibco, 12055-083, RRID: SCR_008452) supplemented with 800 U/mL of recombinant human GM-CSF (Thermo Fisher Scientific, 215-GM) and 500 U/mL of recombinant human IL4 (R&D Systems, 204-IL-050) to generated dendritic cells (DC). DCs were matured with 10 ng/mL of recombinant human TNFγ (R&D Systems, 210-TA), 2 ng/mL of recombinant human IL1β (R&D Systems, 201-LB-005), 1,000 U/mL of recombinant human IL6 (R&D Systems, 206-IL-010), and 1,000 ng/mL of prostaglandin E2 (MP Biomedicals, 219457601). Following maturation, DCs were pulsed with 10 μmol/L of predicted peptides for 4 hours at room temperature and irradiated at 5,000 rad.

Antigen-specific T cells were generated with autologous PBMCs mixed with irradiated, peptide-pulsed DCs at 35:1 ratio cultured in T-cell medium (LymphoOne T-cell expansion medium, Takara, WK552S) supplemented with 5 ng/mL of recombinant human IL7 (R&D Systems, 207-IL-005) and 30 ng/mL of recombinant human IL21 (PeproTech, AF-200-21) for 1 week to enhance growth of antigen-specific T cells. Cultured T cells were restimulated with irradiated, peptide-pulsed DCs as described above. Recombinant human IL2 at 10 U/mL was supplemented every 2 days.

### Isolation of antigen-specific T cells

Tetramers specific to predicted peptides were designed and generated by Baylor MHC Tetramer Production Core, Fred Hutchinson Cancer Research Center, or the National Institute of Health (NIH). Antigen-specific T cells were stained with PE-conjugated tetramer and PB-conjugated anti-CD8 (BD Biosciences Pharmingen, 558207) and sorted for tetramer/CD8 double-positive T cells. Sorted antigen-specific T-cell population was expanded using a rapid expansion protocol (REP) (27). Expanded antigen-specific T cells were further purified by repeating flow cytometry sorting for tetramer/CD8 double-positive T cells.

### Antigen-specific T-cell cytotoxicity assay

The capability of antigen-specific T cells to induce target cell lysis was assessed by chromium-51 ($^{51}$Cr) release assay (28). Briefly, target tumor cells in appropriate growth medium (H1975: RPMI Gibco, 11875-0930; 293: DMEM Corning, 10-013-CV) supplemented with 10% FBS (GenDEPOT, F0601-050) containing 100 μL of $^{51}$Cr were incubated at 37°C for 2 hours. Target tumor cells were washed to remove free chromium and seeded in 96-well U-bottom cell culture plate. Effector T cells from normal donors were added at varying ratios to target tumor cells. Media with only $^{51}$Cr-labeled target cells were used as a negative control ("minimum"). $^{51}$Cr-labeled target cells with lysis buffer (Revvity, 4005-0010) were used as a positive control ("maximum"). The supernatant was periodically collected between 4 and 24 hours of incubation, and chromium released by lysed target tumor cells was measured using a 2450 MicroBeta2 microplate counter (PerkinElmer). The percent of specific lysis was calculated by averaging replicates and using the following equation: [(sample average − minimum average)/(maximum average − minimum average)] × 100.

### Identification of αβTCR chains

Expanded, reactive antigen-specific T cells were processed using 10x Genomics Single Cell 5′ Gene Expression and V(D)J profiling kit and sequenced using Illumina NovaSeq 6000 at Advanced Technology Genomics Core of University of Texas MD Anderson Cancer Center. Raw data were processed through CellRanger pipeline for demultiplexing, alignment, barcode processing, and CDR3 α/β sequence assembly of clonotypes. The clonotypes identified and used for downstream T cell transduction were TCR-1 (HLA-A*02:01 restriction; cognate peptide, YLVPIQFPV; TCRβ, CASSYAGPGELFF), TCR-2 (HLA-A*24:02 restriction; cognate peptide, IYTWIEDHF; TCRβ, CASGTGQLSEQYF), TCR-3 (HLA-A*24:02 restriction; cognate peptide, IYTWIEDHF; TCRβ, CASRSDYNEQFF), and TCR-4 (HLA-A*23:01 restriction; cognate peptide, IYTWIEDHF; TCRβ, CAFRGAPNTGELFF).

### Recombinant TCR retroviral production

Full-length TCRα/β genes were synthesized by GenScript USA, Inc. (RRID: SCR_002891) and cloned into the pMSGV1 retroviral vector as described by the Hughes and colleagues (29). Briefly, TCR constructs were designed with Furin and P2A cleavage to connect TCRα and TCRβ chains for maximum release of TCRα/β chains after expression (30). Viral particles were generated with pMSGV1-TCR construct (GenScript USA, RRID: SCR_002891) and RD114 envelope construct by cotransfection into the retroviral packaging cell line GP2-293 (Takara Bio, 631458, RRID: CVCL_WI48) with Lipofectamine 3000 transfection reagent (Thermo Fisher Scientific, L3000008; ref. 31). Following 48 and 72 hours of transfection, the supernatant was collected, centrifuged, filtered, and used for downstream T-cell transduction.

### Generation of TCR-T cells

HLA-matched fresh leukapheresis products from healthy adult donors ($n$ = 4) from Charles River Company (D79040 and D179395) and AllCells (19384 and 43026) were obtained at FDA-registered collection centers under written informed consent. Healthy donor PBMCs were processed within 48 hours of collection, preserved, and stored in liquid nitrogen. PBMCs were used to isolate CD8$^+$ T cells by negative selection using Human CD8$^+$ T cell Isolation Kit (Stemcell, 17953). Isolated CD8$^+$ T cells were activated by culturing T cells in T-cell medium (LymphoOne T cell expansion medium, Takara, WK552S) with T-cell TransAct (Miltenyi Biotec, 130-111-160) and 100 U/mL of recombinant human IL2 (PeproTech, 200-02-250) for 48 hours. Non–tissue culture–treated 24-well plates were coated with 20 μg/mL of RetroNectin (Takara, T100B) in 4°C overnight. Prior to use, RetroNectin-coated plates were blocked with 2% BSA/PBS for 30 minutes and washed with 2.5% HEPES/PBS. A first TCR-T cell transduction was performed, in which the supernatant collected from the retroviral transfection containing TCR viral particles was added to RetroNectin-coated

plates and centrifuged at 2,000 *g* for 2 hours at 32°C. Unbound viral particles were removed from the 24-well plate. Next, $5 \times 10^5$ activated $CD8^+$ T cells were added to each well and centrifuged at 800 *g* for 20 minutes at 32°C. Cells were incubated overnight in T-cell medium supplemented with 100 U/mL of human recombinant IL2. T-cells were collected, and the process was repeated to perform a second TCR-T cell transduction. After 48 hours, virally transduced TCR-T cells were stained for $CD8^+$ and tetramer, and double-positive populations were isolated by flow cytometry sorting. Sorted TCR-T cells were expanded in T-cell medium supplemented with 300 U/mL of human recombinant IL2 in G-Rex 24-well plates (Wilson Wolf, 80192M) for 4 to 8 days.

### TCR-T cell–mediated cytotoxicity and reactivity

Cytotoxicity and specificity toward target tumor cell lines mediated by antigen-specific TCR-T cells were analyzed by chromium-51 release assay, as described above. Briefly, target cell lines were peptide pulse by incubating relevant peptides (GenScript USA, Inc.) for 2 hours at 37°C in PBS supplemented with 1% FBS (GenDEPOT, F0601-050) and washed with T-cell medium. Specificity of TCR-T cells were evaluated by the titration of peptides at varying concentrations ($10^{-2}$ to $10^4$ nmol/L) in the presence of chromium-51. Target cells were seeded in 96-well plates and cocultured with TCR-T cells at a 1:1 ratio for 8 to 24 hours. $EC_{50}$ values were calculated using GraphPad Prism (GraphPad). FOXM1-specific TCR-T1 were cocultured for 24 hours with HLA-A*02:01-expressing normal cells lines. Reactivity of FOXM1 TCR-T cells was then measured by LDH release assay (Cayman Chemical Company, 601170) and MIP-1β secretion (R&D Systems, DY27105).

### Cytokine assessment

To determine the reactivity of TCR-T cells toward target tumor cell lines, IFNγ Enzyme-linked ImmunoSpot (ELISPOT) and secretion of MIP-1β (DuoSet Human CCL4/MIP-1β ELISA Kit; R&D Systems, DY271) were measured (32). For these assays, TCR-T cells were cocultured with unmatched HLA tumor cells, FOXM1/matched HLA-transduced tumor cells, or peptide-pulsed tumor cells for 15 to 18 hours. TCR-T cells were cocultured at a 1:1 ratio for ELISPOT methods. ELISPOT plates were scanned and counted using ImmunoSpot ELISPOT analyzer (Cellular Technology, Ltd). TCR-T cells were cocultured at a 1:1, 0.5:1, and 0.25:1 target to effector ratio for MIP-1β ELISA methods and analyzed according to the manufacturer's instructions. MIP-1β ELISA methods were also utilized for endogenous recognition of DFCI032 and MDA-L-30 cell lines and X-scanning. Briefly, corresponding target tumor cells were individually peptide-pulsed with modified peptides containing a single amino acid substituted in each position (10 μg/mL; GenScript USA, Inc.) for 4 hours, cocultured with TCR-T cells at a 5:1 target-to-effector ratio, and ELISA plates were read with Synergy microplate reader (BioTek) using Gen5 program. Concentration of MIP-1β for samples was calculated according to the standard curve.

### Time-lapse flow cytometric assessment

FOXM1 TCR-T cells were thawed and rested overnight in RPMI-1640 cell culture medium containing 10% (v/v) FBS, 1% (v/v) sodium pyruvate, 1% (v/v) NEAA, 55 nmol/L 2-mercaptoethanol, and 1% (v/v) penicillin/streptomycin (P/S) at 37°C with 5% $CO_2$. The following morning, cells were barcoded with biotin-coated LASE particles (LP) and stained with Live/Dead stain (Zombie R718, BioLegend, 423115), followed by a panel of releasable anti–CD8-VioGreen (Miltenyi Biotec, 130-115-197), anti–CD45RA-FITC (Miltenyi Biotec, 130-112-079), and anti–PD-1-PE-Vio770 (Miltenyi Biotec, 130-119-921; ref. 33). For phenotyping, cells were additionally stained with anti–CCR7-Brilliant Violet 650 (BioLegend, 353233), anti–CD45RO-APC (BioLegend, 983102), anti–LAG-3-APC-Fire 750 (BioLegend, 369329), and anti–TIM-3-PE-Fire 700 (BioLegend, 345063). Samples were run on the cyclic flow cytometer, collected, and then resuspended in 1% (v/v) of release reagent (Miltenyi Biotec, 130-120-675) for 10 minutes at room temperature to remove the releasable antibody panel (33). Next, the cells were stimulated with 10 μg/mL either of specific (FOXM1) or nonspecific peptide in the presence of 1 μg/mL costimulatory antibodies (CD28 and CD49d, BioLegend) for 36 hours and restained with the same antibody panel (34–36). All samples were acquired by the cyclic flow cytometer at each time point (LASE Innovation) and returned to their original culture supernatants. FCS files from each cyclic measurement (e.g., before and after activation with peptides) were concatenated by LP barcode using the LP matching algorithm as described previously (33).

### Structural modeling

Structural models for the TCR–pMHC complexes were generated using TCRmodel 2 with the default parameters referencing AlphaFold2.3 (37, 38). First, three-dimensional conformations generated by TCRmodel2 with incident angles ranging between 0 and 45 degrees or crossing angles between 5 and 95 degrees were considered, based on previously reported cutoff values (bioRxiv 2024.05.27.596020; ref. 39). Next, conformations with the highest PLDDT score produced by AlphaFold2.3 for each TCR-pMHC complex were selected.

### Animal experiments

Animal experiments were conducted under the Institutional Animal Care and Use Committee–approved protocol (#00002019-RN01). NOD.Cg-*Prkdc*$^{scid}$ *Il2rg*$^{tm1Wjl}$/SzJ (NSG) mice were purchased from The Jackson Laboratory (The Jackson Laboratory, 005557). Six-week-old female mice were subcutaneously injected into the right flank with $0.5 \times 10^6$ H1975 FOXM1 (HLA-A*02:01) tumor cells. Mice were randomized into three groups: FOXM1 TCR-T cell treatment, untransduced T cells, and PBS control ($n = 10$ for each group) when tumors were established to ~50 $mm^3$. Measurements of tumor width and diameter with digital calipers [volume = $(\text{minimum})^2 \times (\text{maximum})/2$], as well as animal weights, were recorded by a blinded investigator at baseline and three times weekly thereafter. Ten million TCR-T1 cells were intravenously transfused via retro-orbital injection on days 4 and 7. Control groups received an equal number of untransduced $CD8^+$ T cells from the same HLA-A*02:01 donor or PBS. Mice simultaneously received IL15/IL15Rα complex intraperitoneally every 3 days for the duration of the experiment, beginning at the time of the first T-cell injection (40). Peripheral whole blood was collected longtudinally from murine models on days 10 and 23 via retro-orbital bleeding. At the time of sacrifice, tumor and whole blood by cardiac puncture were collected. At the time of collection, whole blood was prepared, stained for anti-CD8 APC (BioLegend, 344722) and tetramer PE, and measured by flow cytometry. For survival analyses, mice sacrificed because of tumor ulceration rather than tumor burden were censored.

### Statistical analysis

All statistical analyses were performed using GraphPad Prism v10.0.3 (GraphPad Software, RRID: SCR_002798). Two-way ANOVA

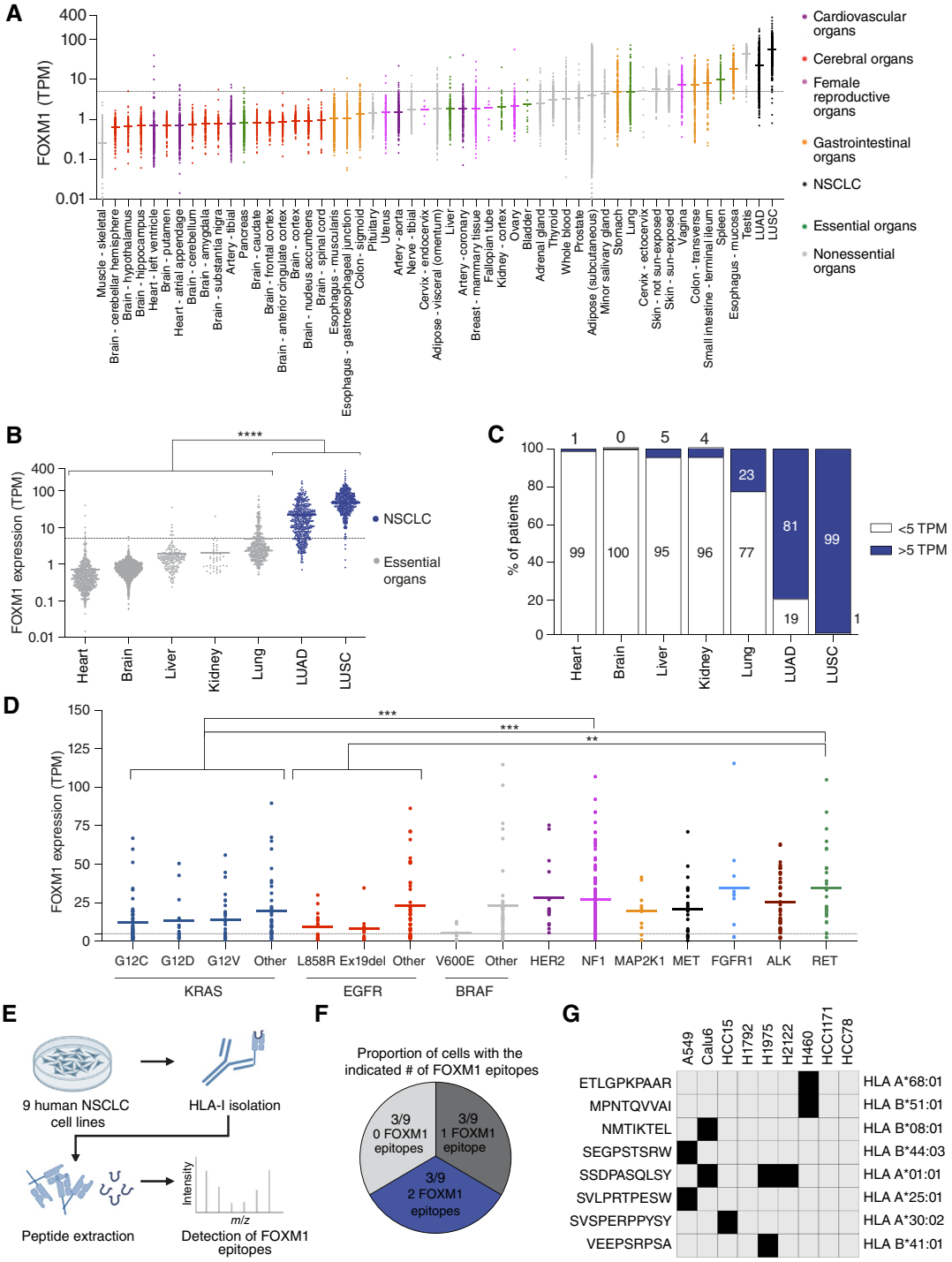


**Figure 1.**

FOXM1 expression is induced in lung cancers vs. healthy human tissues. **A,** RNA expression data of FOXM1 in patients with lung cancer obtained from TCGA and healthy tissues. Five TPM cutoff is marked. **B,** FOXM1 RNA expression in essential organs compared with lung cancer samples. Five TMP cutoff is indicative of FOXM1 positivity. **C,** Percentage of patients with FOXM1-positive expression in essential organs compared with lung cancer. **D,** RNA expression data of nonmetastatic lung cancer patient samples obtained from TCGA grouped by mutation type. Five TPM cutoff is marked. **E,** Experimental overview for immunopeptidomics. **F,** Pie chart depicting the proportion of NSCLC cell lines presenting FOXM1 epitopes and (**G**) eluted epitopes and HLAs from each cell line. Bars represent mean and each dot represents a single patient sample. **, $P < 0.01$; ***, $P < 0.001$; ****, $P < 0.0001$ using one-way ANOVA. [**E,** Created in BioRender. Bontekoe, E. (2026) https://BioRender.com/9bnwhqv]

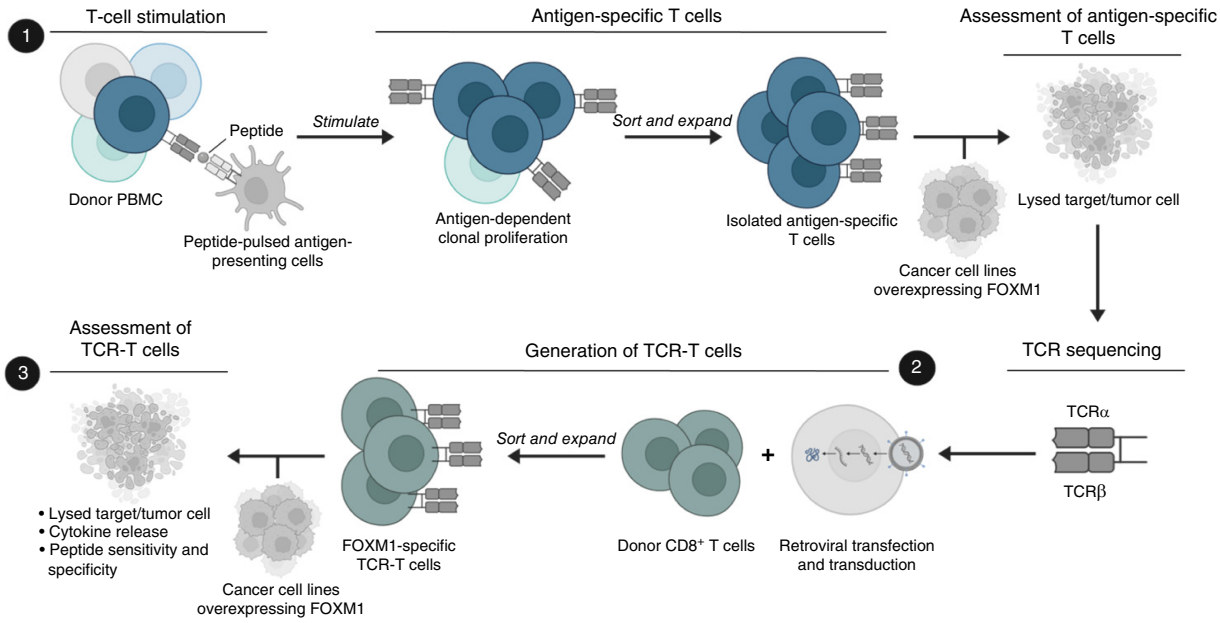


**Figure 2.**

Generation of antigen-specific T cells targeting FOXM1. Overview of T-cell generation workflow. DCs are pulsed with defined peptides and used to stimulate antigen-specific T-cell expansion. After tetramer sorting and expansion, TCR α/β pairs are identified by single-cell TCR/RNA sequencing and cloned into a retroviral vector. TCRs are transduced into healthy donor PBMCs for further functional validation. [Created in BioRender. Bontekoe, E. (2026) https://BioRender.com/mmp9o4o]

and paired or unpaired *t* test were performed when appropriate based on data types and statistical assumptions. Significance was defined as $P$ value < 0.05. TCR repertoire analysis was performed by utilizing UMAP and GLIPH2 clustering. Graphs were generated with GraphPad Prism. Some schematics were created using BioRender (RRID: SCR_018361).

## Results

### FOXM1 is prevalent in lung cancer and minimally expressed in healthy organs and tissues

To evaluate FOXM1 in NSCLC, RNA expression from TCGA was compared with normal tissue transcript expression from GTEx. As shown in **Fig. 1A**, FOXM1 expression was increased in lung adenocarcinoma (LUAD, $n = 517$) and lung squamous cell carcinoma (LUSC, $n = 501$), with average expression of 22.49 TPM in LUAD and 56.62 TPM in LUSC. Conversely, overall healthy tissues averaged 4.04 TPM. Based on prior studies, a >5 TPM cutoff was used to identify samples positive for FOXM1 expression (41). Using this threshold, FOXM1 RNA expression in essential organs was assessed (heart, $n = 600$; brain, $n = 1{,}671$; liver, $n = 175$; kidney, $n = 45$; and lung, $n = 427$). Compared with NSCLC, all essential organs expressed markedly lower FOXM1 expression and fell below the 5 TPM threshold (brain, 0.79 average TPM, $P < 0.0001$; heart, 0.71 average TPM, $P < 0.0001$; kidney, 2.07 average TPM, $P < 0.0001$; liver, 1.88 average TPM, $P < 0.0001$; and lung, 4.99 average TPM, $P < 0.0001$, **Fig. 1B**). Specifically, FOXM1 was absent in 99% of heart samples ($n = 594$), 100% of brain samples ($n = 1{,}671$), 95% of liver samples ($n = 1{,}670$), 96% of kidney samples ($n = 44$), and 77% of lung samples ($n = 329$). In contrast, 81% of LUAD ($n = 419$) and 99% of LUSC ($n = 496$) tumors expressed FOXM1 (**Fig. 1C**). Analysis of FOXM1 protein expression using the Human Protein Atlas revealed elevated levels in lung cancer, with minimal expression in normal tissue (Supplementary Fig. S1A), which was further confirmed by Western blot analysis in five essential normal tissue cell lines (Supplementary Fig. S1B). A positive correlation between protein and mRNA expression was also observed (Supplementary Fig. S1C). Given the observed upregulation of FOXM1 in NSCLC and minimal expression in normal tissue, we further investigated its expression across mutational subtypes using TCGA datasets. Notably, FOXM1 expression was elevated in tumors harboring Ret alterations compared with KRAS and EGFR mutations ($P = 0.005$; **Fig. 1D**). To evaluate whether the widespread expression of FOXM1 in lung cancer resulted in presentation of FOXM1 epitopes on HLA molecules, we performed immunopeptidomics on nine NSCLC cells lines (**Fig. 1E**). We found that two thirds displayed endogenous presentation of one or two FOXM1-derived epitopes across distinct HLA alleles, highlighting the broad potential for FOXM1 as an HLA-restricted TAA (**Fig. 1F** and **G**).

### FOXM1 is immunogenic on HLA-A*02:01 and HLA-A*24:02

Building upon these initial findings, we sought to identify circulating FOXM1-specific T cells. In doing so, we developed an optimized TCR discovery and validation workflow which allows us to identify, isolate, and validate antigen-specific T cells and their T-cell receptors (**Fig. 2**). Briefly, healthy donor T cells are cocultured with antigen-presenting cells pulsed with predicted peptides to simulate antigen-specific responses. These stimulated T cells are then enriched and expanded. Cytotoxicity of these T cells against tumor cell lines is evaluated to ensure target epitopes are naturally endogenously processed and presented, and αβTCR chains are sequenced to identify the reactive TCRs. TCR-T cells are generated by

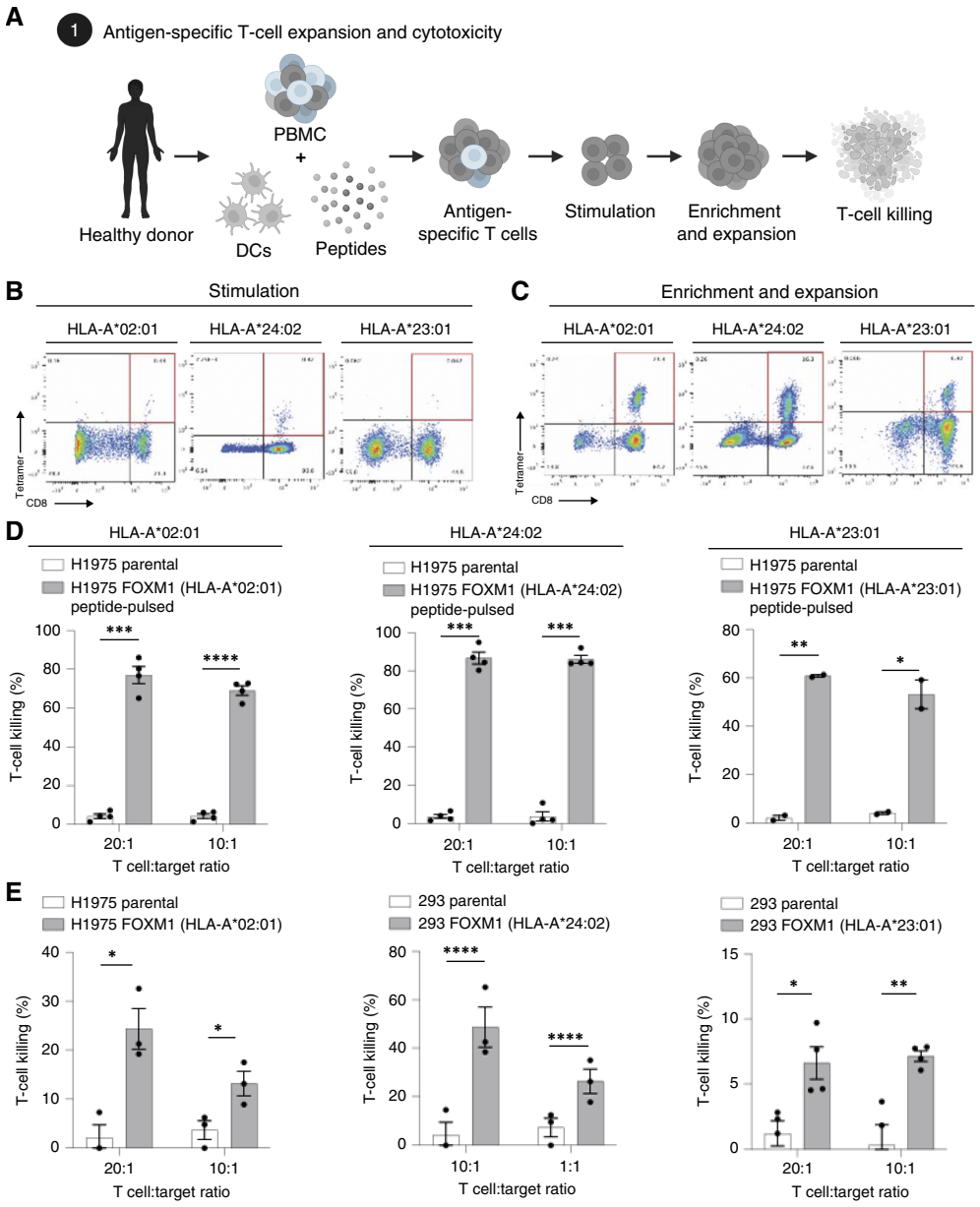


**Figure 3.**

FOXM1 antigen-specific T cells exhibit cytotoxic potential. **A,** Schematic representation for the identification of antigen-specific T cells. Patient and/or donor PBMCs are isolated and cocultured with DCs peptide pulsed with target antigen for the generation of antigen-specific T cells. Antigen-specific T cells are stimulated, enriched, and expanded. Cytotoxicity of antigen-specific T cells toward tumor cell lines is assessed. **B** and **C,** Stimulation, enrichment, and expansion of antigen-specific T cells following FOXM1 peptide stimulation on HLA-A*02:01, HLA-A*24:02, and HLA-A*23:01. Samples were identified and isolated by CD8/tetramer sorting. Red gate represents sorted cell population used for subsequent assays. Chromium-51 release assay of expanded FOXM1-specific T cells cocultured with peptide-pulsed (**D** and **E**) unpulsed HLA-matched cell lines. Bars represent mean values ± SEM, and each dot represents a technical replicate. At least two technical replicates were included for each experiment. *, $P < 0.05$; **, $P < 0.01$; ***, $P < 0.001$; ****, $P < 0.0001$ using unpaired $t$ test. [**A,** Created in BioRender. Bontekoe, E. (2026) https://BioRender.com/mmp9o4o]

retroviral transduction using healthy donor PBMCs, and the cytotoxicity of TCR-T cells is subsequently assessed to confirm antitumor reactivity and specificity (**Fig. 2**). To identify high-potential FOXM1-derived epitopes for immunotherapeutic development, we systemically surveyed published studies surrounding FOXM1 and prioritized the *YLVPIQFPV* and *IYTWIEDHF* epitopes based on their previously reported immunogenicity (42–45). We next utilized NetMHCpan4.1 to predict peptide binding to the 10 most prevalent HLA alleles in the United States (14, 43). As shown in Supplementary Table S1, these peptides were predicted to bind to HLA-A*02:01 and HLA-A*24:02 (*YLVPIQFPV*, HLA-A*02:01, 2.11 nmol/L; *IYTWIEDHF*, HLA-A*24:02, 34.26 nmol/L). The

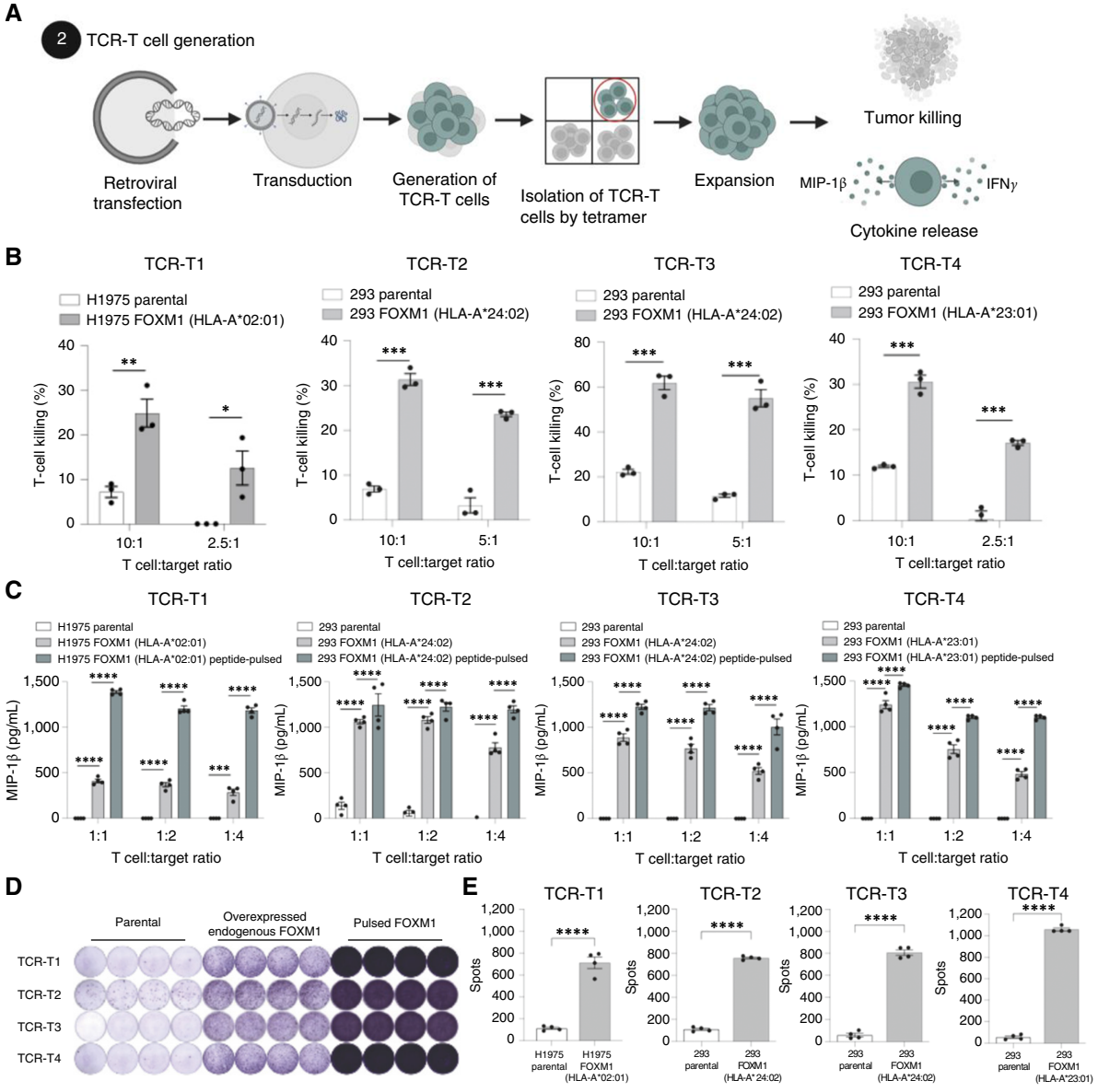


**Figure 4.**

TCR-engineered T cells exhibit cytotoxicity toward FOXM1. **A,** Schematic representation of TCR-T cell generation. Antigen-specific T cells are sequenced, and TCRs are retrovirally transduced into donor CD8 T cells. Generated TCR-T cells are sorted by CD8/tetramer, isolated, expanded, and analyzed for activation and cytotoxic potential toward target tumor cells. **B,** Cytotoxicity of FOXM1 TCR-T cells by chromium-51 release toward parental or HLA-matched target cell lines. Cytokine release of TCR-T cells measured by (**C**) MIP-1β and (**D, E**) IFNγ following coculture with parental, HLA-matched, or peptide-pulsed HLA-matched target cell lines. Bars represent mean values ± SEM, and each dot represents a technical replicate. At least three technical replicates were included for each experiment. *, $P < 0.05$; **, $P < 0.01$; ***, $P < 0.001$; ****, $P < 0.0001$ using unpaired *t* test. [**A,** Created in BioRender. Bontekoe, E. (2026) https://BioRender.com/mmp9o4o]

*IYTWIEDHF* epitope was also predicted to bind to the HLA-A*23:01 allele (31.62 nmol/L), which is less prevalent in the United States. In our cell lines of interest [H1975, H1975 (HLA-A*02:01), and H1975 FOXM1 (HLA-A*02:01), Supplementary Fig. S2A], the eluted epitopes were primarily 9-mers, consistent with expected class I HLA-binding preferences (Supplementary Fig. S2B). Across these peptides, we defined position-specific amino acid abundance and identified dominant residues at key anchor positions, in line with HLA restriction of these epitopes (Supplementary Fig. S2C and S2D). Notably, the FOXM1 epitope of interest was detected among the eluted peptides from H1975 FOXM1 (HLA-A*02:01) cells, confirming its endogenous processing and presentation in this model (Supplementary Fig. S2E and S2F).

We proceeded to stimulate PBMCs from HLA-A*02:01, HLA-A*24:02, and HLA-A*23:01 healthy donors with each of these peptides to confirm their immunogenicity via antigen-specific T-cell expansion (**Fig. 3A**). FOXM1-specific T-cell populations were detected in all three HLA contexts following stimulation at frequencies

ranging from 0.04% to 0.4% (**Fig. 3B**). Tetramer and CD8 double-positive T cells were then isolated for subsequent REP, resulting in 6.9% to 21.3% tetramer positivity (**Fig. 3C**). Functional potential of antigen-specific T cells was next evaluated by assessing cytotoxicity against FOXM1 by chromium-51 release. As shown in **Fig. 3D**, a 10:1 effector-to-target (E:T) ratio resulted in lysis of 69% (HLA-A*02:01, $P < 0.0001$), 86% (HLA-A*24:02, $P = 0.0002$), and 53% (HLA-A*23:01, $P = 0.0836$) of FOXM1 peptide-pulsed target cells. Most importantly, this E:T ratio also resulted in antigen-dependent lysis of target cells endogenously processing and presenting the FOXM1 gene on HLA-A*02:01 ($P = 0.0382$), HLA-A*24:02 ($P < 0.0001$), and HLA-A*23:01 ($P = 0.0053$; **Fig. 3E**). These findings confirm that FOXM1 epitopes are not only immunogenic but naturally endogenously processed and presented on HLA-A*02:01, HLA-A*24:02, and HLA-A*23:01.

### TCR-T cells exhibit cytotoxic potential against FOXM1-expressing targets

To generate TCR-T cells, we performed single-cell TCR/RNA sequencing on tetramer-sorted populations to identify αβTCR pairings, and the dominant T-cell clonotypes were assessed and selected for downstream generation of TCR-T cells (Supplementary Fig. S3A and S3B). The αβTCRs were synthesized and subcloned into retroviral vectors for transduction into HLA-matched healthy donor PBMCs. Successfully transduced TCR-T cells were isolated by tetramer sorting and expanded by REP (Supplementary Fig. S4A). TCR-T cells were then exposed to their cognate antigens for the assessment of cytotoxicity, cytokine production, and phenotype following antigen exposure (**Fig. 4A**). Of the screened TCRs for each HLA/target, TCR-T1 (HLA-A*02:01), TCR-T2 (HLA-A*24:02), TCR-T3 (HLA-A*24:02), and TCR-T4 (HLA-A*23:01) demonstrated cytotoxicity toward HLA-matched cell lines compared with nontransduced parental cell lines at varying E:T ratios (**Fig. 4B**). As shown in **Fig. 4B**, TCR-T cells lysed 25% (TCR-T1, $P = 0.0063$), 31% (TCR-T2, $P < 0.0001$), 62% (TCR-T3 $P = 0.0002$), and 31% (TCR-T4 $P = 0.0002$) of target cells at a 10:1 E:T ratio. TCR-T cells also secreted MIP-1β when cocultured with tumor cells expressing FOXM1 (TCR-T1, $P < 0.0001$; TCR-T2, $P < 0.0001$; TCR-T3, $P < 0.0001$; and TCR-T4, $P < 0.0001$) or peptide-pulsed (TCR-T1, $P < 0.0001$; TCR-T2, $P = 0.0001$; TCR-T3, $P < 0.0001$; and TCR-T4, $P < 0.0001$) at E:T ratios as low as 0.25:1 (**Fig. 4C**). Similarly, TCR-T cells secreted IFNγ as measured by ELISpot when exposed to cognate antigen (TCR-T1, $P < 0.0001$; TCR-T2, $P < 0.0001$; TCR-T3, $P < 0.0001$; and TCR-T4, $P < 0.0001$, **Fig. 4D** and **E**). When assessing the phenotype of FOXM1 TCR-T1 cells, a predominantly effector memory (TEM) phenotype was observed, comprising of approximately 80% of the population (Supplementary Fig. S4B). Additionally, upon stimulation with cognate peptide for 36 hours, 2.5% to 4% TCR-T1 cells exhibited a terminally differentiated effector memory T cell (TEMRA) phenotype ($CD45RA^+$ $CCR7^-$ $CD45RO^-$), and 35% of TCR-T1 cells coexpressed checkpoint molecules ($TIM\text{-}3^+LAG\text{-}3^+PD\text{-}1^+$) despite initial lack of expression (Supplementary Fig. S4C). Lastly, we performed time-lapse flow cytometric assessment of TCR-T1 to evaluate activation profiles based on CD25 and CD69 expression. As shown in Supplementary Fig. S4D, *de novo* activation was specific to cognate peptide exposure, as evidenced by 17% of TCR-T1 cells (devoid of CD25 and CD69 at baseline) expressing these activation markers 12 hours after stimulation. These analyses highlight the phenotype and activation kinetics of TCR-T cells prior to and following antigen exposure.

### FOXM1-specific TCR-T cells are unresponsive to healthy organs

Cytokine production and cytotoxicity of TCR-T1 toward healthy tissue cell lines were assessed to determine possible on-target, off-tumor toxicities (Supplementary Fig. S5). First, we determined healthy tissue cell lines' endogenous HLA restriction and confirmed none expressed HLA-A*02:01 (Supplementary Fig. S5A). Therefore, each cell line was transduced with HLA-A*02:01 (Supplementary Fig. S5B). TCR-T1 demonstrated significantly less secretion of MIP-1β when cocultured with each HLA-matched healthy tissue cell line compared with an average of 311.7 pg/mL in response to the target tumor cell line ($P < 0.0001$; Supplementary Fig. S5C). TCR-T1 additionally demonstrated an average lysis of 1.6% of lung ($P < 0.0001$), 2.1% liver ($P < 0.0001$), 0% heart ($P < 0.0001$), 0% kidney ($P < 0.0001$), and 0% brain ($P < 0.0001$) compared with 32.7% lysis of H1975 FOXM1 (HLA-A*02:01) (Supplementary Fig. S5C). Consistent with these findings, Western blot analysis demonstrated low FOXM1 expression in essential organ cell lines compared with robust FOXM1 expression in tumor cell lines transduced with FOXM1 (Supplementary Fig. S1B). Altogether, these results suggest that FOXM1 TCR-T cells become activated upon recognition of their cognate antigens while sparing healthy tissues.

### FOXM1-specific clonotypes are detected in patients with lung cancer

We next sought to assess the existence of FOXM1-specific clonotypes in lung cancer patient samples. To do so, we obtained a leukapheresis from a patient homozygous for HLA-A*23:01 and performed peptide stimulations using the validated *IYTWIEDHF* epitope. As shown in **Fig. 5A**, despite a low precursor frequency of 0.19%, FOXM1-specific clonotypes were expanded to 82.9% upon REP. Most importantly, these cells demonstrated functional potential through their ability to secrete IFNγ as measured by ELISpot ($P < 0.0001$; **Fig. 5B**). To further expand our analysis, we evaluated TCR motifs related to validated FOXM1-specific TCRs with the grouping of lymphocyte interactions by paratope hotspots (GLIPH) algorithm using CDR3β sequencing data from the ICON ($n = 104$) and PROSPECT ($n = 275$) cohorts. As shown, TCRs related to TCR-T1, TCR-T2, and TCR-T4 were prevalent across each of these cohorts (**Fig. 5C**). All in all, these data establish that FOXM1-specific clonotypes are not restricted to healthy individuals but also arise naturally in patients with lung cancer.

### FOXM1-specific TCR-T cells are sensitive and specific

We next evaluated the sensitivity and specificity of FOXM1-targeted TCR-T cells (**Fig. 6A**). As demonstrated in **Fig. 6B**, sensitivity was evaluated through peptide titration by chromium-51 release assay, in which TCR-T cells exhibited cytotoxicity in the presence of specific FOXM1 epitopes at a log $EC_{50}$ value ≤1.4 nmol/L (TCR-T1, 1.4 nmol/L; TCR-T2, 1.3 nmol/L; TCR-T3, 1.0 nmol/L; and TCR-T4, 0.2 nmol/L). We further generated structural modeling of TCR–peptide–HLA complexes to visualize TCR contact residues. Structural modeling revealed key TCR recognition sites within the central region of the peptides for positions P1, P4, P5, P6, and P7 for TCR-T1 (**Fig. 6C**) and positions P4, P6, and P7 for TCR-T2 (Supplementary Fig. S6A). To expand upon these results, we next assessed specific residues of the cognate epitopes by X-scan (**Fig. 6D**). Overall diminished MIP-1β secretion was seen for HLA-A*02:01 when residues

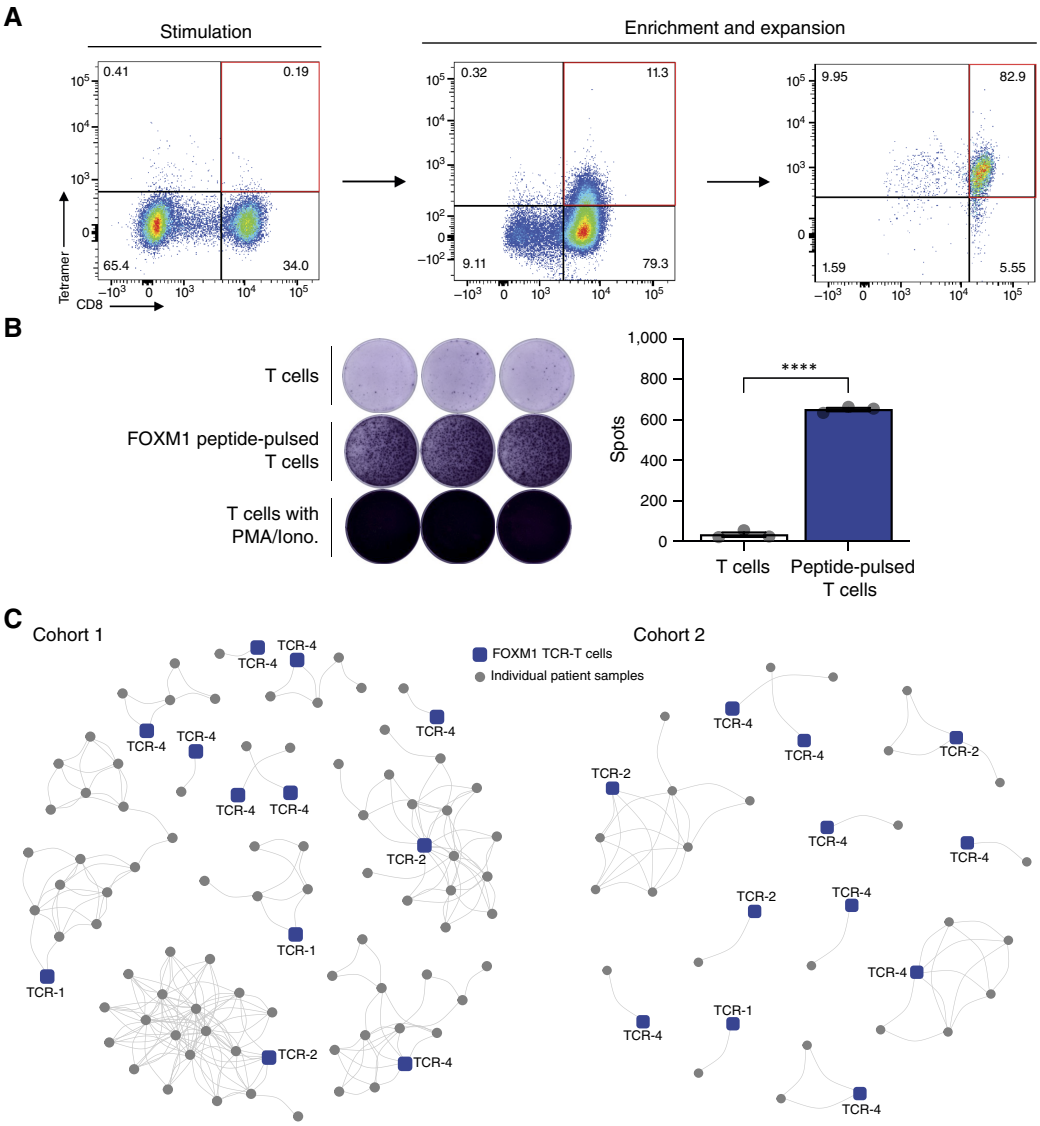


**Figure 5.**

FOXM1-specific and related TCR motifs are identified in patients with lung cancer. **A,** Stimulation, enrichment, and expansion of CD8/tetramer-positive FOXM1-specific T cells in NSCLC patient PBMCs with HLA-A*23:01 restriction. Red gate represents sorted cell population used for subsequent assays. **B,** FOXM1-specific T cells isolated from NSCLC patient sample were peptide-pulsed or pulsed with cell activation cocktail and cytokine secretion was measured by IFNγ release. Bars represent mean values ± SEM, and each dot represents a technical replicate. Three replicates were performed. **C,** GLIPH2 analysis demonstrating patient T cells related to FOXM1 TCR-T cells in ICON (cohort 1) and PROSPECT (cohort 2) patient tumor samples. Each circle represents an individual patient tumor sample and FOXM1 TCR-T cells are denoted as a blue box. PMA/Iono. (PMA/ionomycin), ****, $P < 0.0001$ using unpaired *t* test. PMA/Iono, phorbol 12-myristate 13-acetate/ionomycin.

P5-P8 were mutated to an alternative animo acid. Similarly for TCR-T2, diminished MIP-1β secretion was observed in residues P4-P7 when mutated to an alanine (Supplementary Fig. S6B). These data identify critical residues for the recognition by TCR-T cells. We next evaluated the sensitivity of FOXM1 TCR-T1 cells against HLA-A*02:01-restricted tumor cell lines to assess ability to respond to endogenous levels of FOXM1. As shown in **Fig. 6E**, TCR-T1 cells were capable of specifically recognizing endogenously expressing HLA-A*02:01 tumor cell lines based on MIP-1β secretion in response to both DFCI032 and MDA-L-30 cancer lines. Our findings collectively demonstrate that FOXM1 TCR-T cells exhibit high sensitivity and specificity toward their epitopes.

### FOXM1 TCR-T cells result in prolonged survival *in vivo*

Lastly, we sought to explore *in vivo* efficacy. To do so, we implanted 0.5 million H1975 FOXM1 (HLA-A*02:01) tumor cells subcutaneously in NOD/SCID gamma (NSG) mice. Mice were then treated with two infusions of PBS, untransduced T cells (10 million), or FOXM1 TCR-T1 cells (10 million), and T-cell persistence, tumor burden, animal weight, and survival were monitored (**Fig. 7A**; Supplementary Fig. S7). FOXM1 TCR-T cells

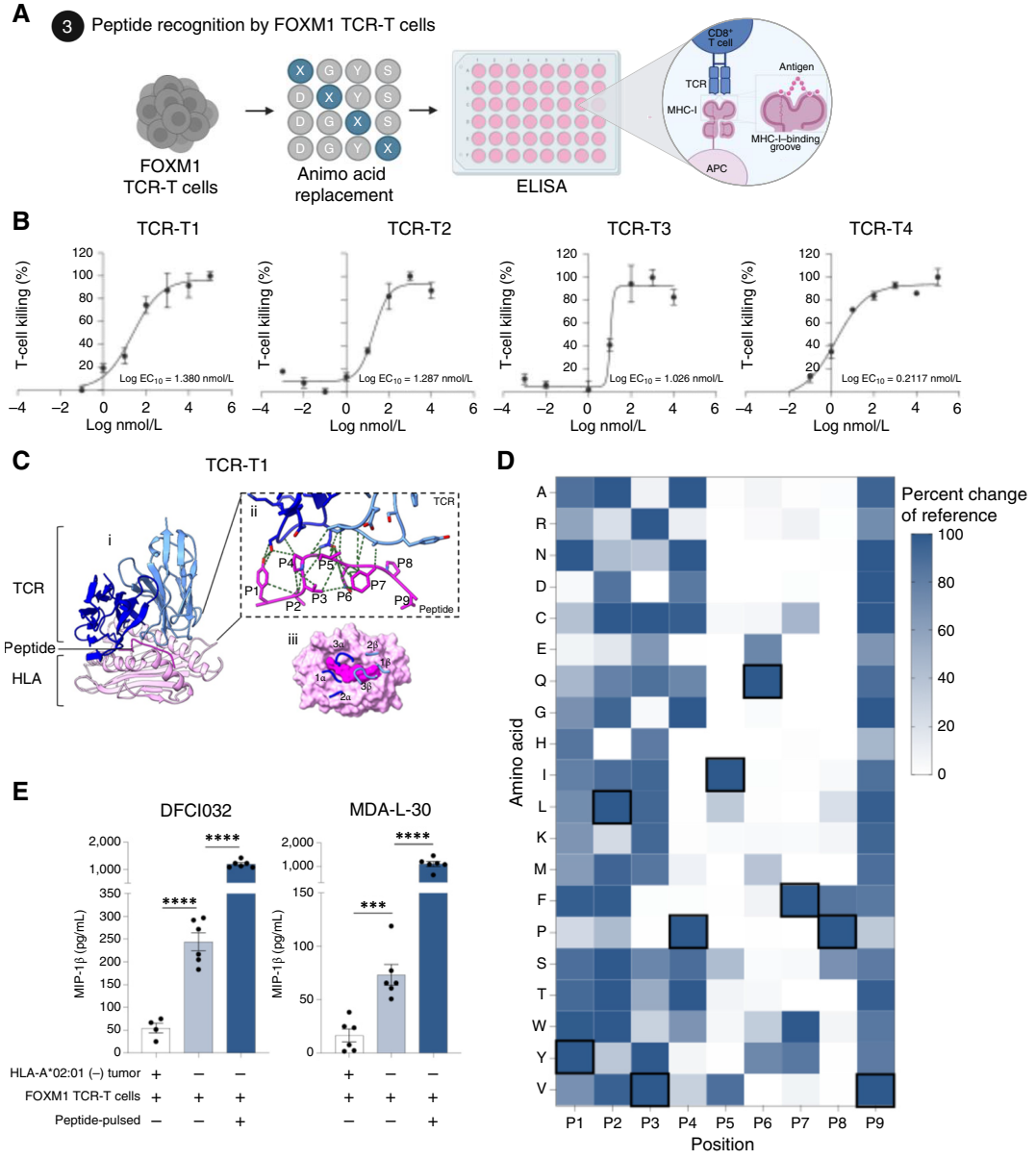


**Figure 6.**

FOXM1-directed TCR-T cells are sensitive and specific. **A,** Schematic representation of amino acid replacement for FOXM1 TCR-T cells. **B,** Peptide titration measured by chromium-51 release assay. Each dot represents a sample ± SEM. **C,** *In silico* modeling of the TCR–T1–pHLA complex. **D,** Critical contacting residues are assessed by sequential amino acid replacement. MIP-1β secretion was measured following coculture of TCR-T1 cells. Heatmap representing percent change in TCR-T cell recognition based on reference peptide after amino acid replacement. Black box indicates unmutated peptide amino acids. Four replicates were performed. **E,** MIP-1β secretion was measured following coculture of TCR-T1 cells with NSCLC tumor cells lines (DFCI032 and MDA-L-30) that endogenously express HLA-A*02:01 and FOXM1. Bars represent mean values ± SEM, and each dot represents a technical replicate. A minimum of four replicates were performed and are representative of three individual experiments are shown. ***, $P < 0.001$; ****, $P < 0.0001$ using unpaired t test. [**A,** Created in BioRender. Bontekoe, E. (2026) https://BioRender.com/mmp9o4o]

significantly reduced tumor burden ($P < 0.0001$) compared with untransduced T cells and untreated mice (**Fig. 7B** and **C**). Furthermore, FOXM1 TCR-T cell–treated mice exhibited significantly prolonged survival compared with those treated with untransduced T cells (**Fig. 7D**). As shown in **Fig. 7E** and **F** and Supplementary Figs. S8 and S9, TCR-T cells were detectable in the periphery on days 10 and 23 and at the time of sacrifice. These results confirm the potential of FOXM1-specific TCR-T cells in combatting lung cancer tumor *in vivo*.

## Discussion

In this study, we evaluated the feasibility of targeting FOXM1 by TCR engineering for the treatment of lung cancer. Our

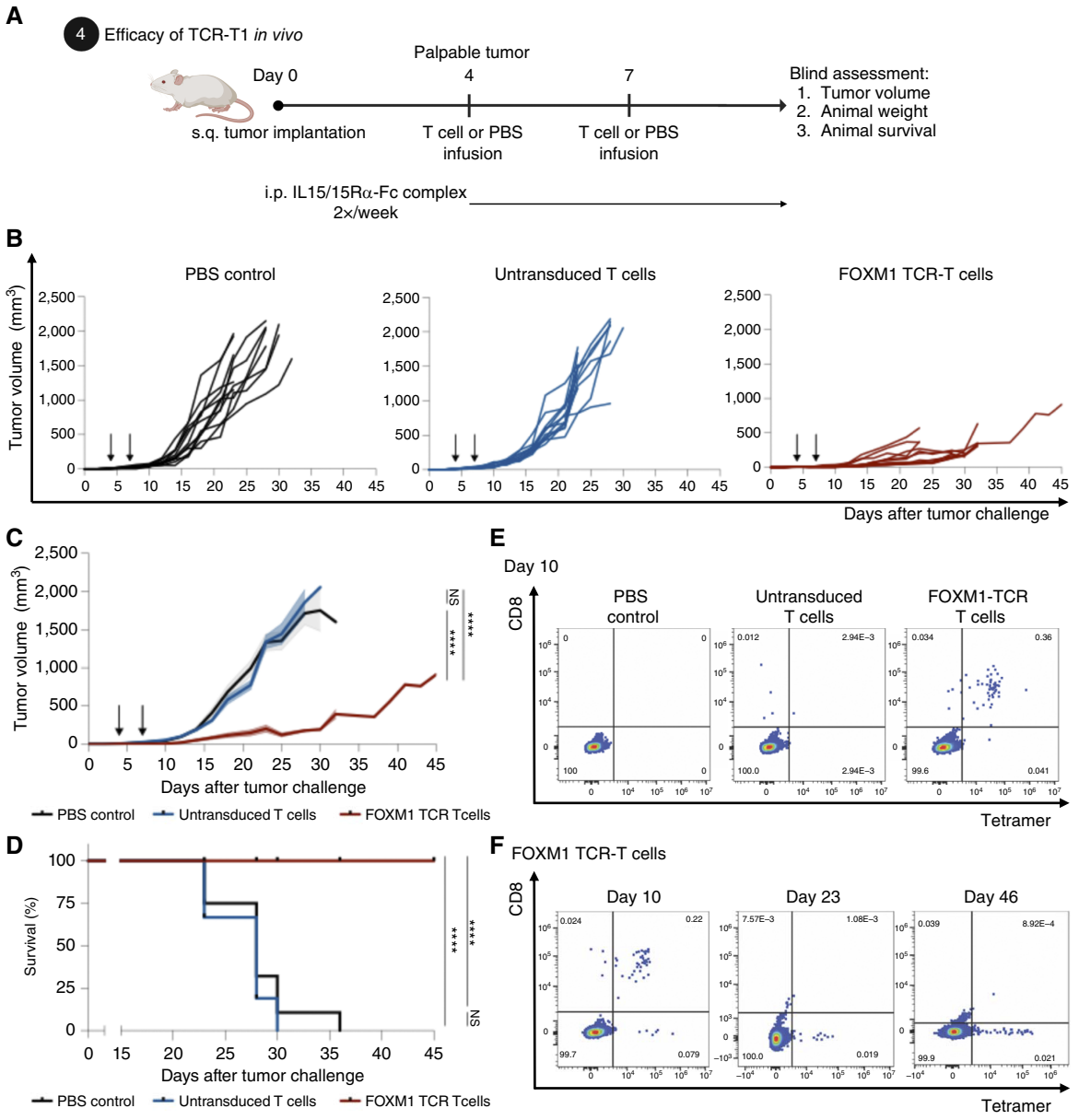


**Figure 7.**

FOXM1-targeting TCR-T cells reduce tumor growth and prolong survival *in vivo*. **A,** Experimental overview for the evaluation of *in vivo* antitumor efficacy of TCR-T1. Mice were randomized into PBS ($n = 10$), untransduced T cells ($n = 10$), or TCR-T1 ($n = 10$) treatment groups once subcutaneous tumors were palpable and intravenously dosed with PBS, $10 \times 10^6$ TCR-T1 cells or untransduced T cells on days 4 and 7. All mice received twice-weekly intraperitoneal injection of IL15/IL15Rα complex starting on the day of T-cell transfer. Tumor volumes (**B** and **C**) and overall survival (**D**). Arrows indicate time of T-cell or PBS infusions. **E,** Representative flow cytometry of $CD8^+tetramer^+$ T cells in indicated treatment groups collected from murine whole blood on day 10. **F,** Longitudinal flow cytometry of $CD8^+tetramer^+$ TCR-T1 cells in whole blood from FOXM1 TCR-T1–treated mouse. Representative of two individual experiments are shown. NS, not significant; ****, $P < 0.0001$ using two-way mixed-effects ANOVA. [**A,** Created in BioRender. Bontekoe, E. (2026) https://BioRender.com/23d37h0]

analyses of TCGA public data demonstrated an increase in FOXM1 expression in lung cancer compared with healthy organs and tissues. Using our validated TCR generation pipeline, we discovered and validated four TCRs specific for epitopes derived from FOXM1 and restricted to HLA-A*02:01, HLA-A*24:02, and HLA-A*23:01. We demonstrated that T cells recognize endogenously expressed FOXM1 via the YLVPIQFPV and IYTWIEDHF epitopes. Functional studies confirmed that TCR-T cells were specific, sensitive, and resulted in cytotoxic responses against FOXM1-expressing cell lines.

Advancements in immunotherapies have highlighted the potential of targeting specific cancer antigens to drive more precise and effective treatments (46). In a phase I clinical trial, 89% of HLA-A*02:01 patients with cervical cancer vaccinated with a 5-peptide cocktail vaccine (containing YLVPIQFPV) exhibited FOXM1-specific T-cell responses as measured by IFNγ secretion (45). However, due to

minimal clinical efficacy and limited immunogenicity often observed with cancer peptide vaccines, further clinical development was not pursued. Additional studies have targeted FOXM1 using small-molecule inhibitors, such as STL001, which induces the translocation of FOXM1 from the nucleus to the cytoplasm, leading to degradation via autophagy and reduced protein expression (47). Other inhibitors, such as XST-20, directly bind the FOXM1 DNA-binding domain and block the regulation of downstream genes essential for cancer cell proliferation (48). Despite these targeted approaches, the clinical utility of small-molecule inhibitors has been limited by issues with specificity, resistance, and underwhelming efficacy (49). In contrast, TCR-T cells may provide potent and persistent targeting of FOXM1-expressing cancer cells, although this strategy carries risks such as cytokine release syndrome and off-target toxicities. Whereas previous studies have demonstrated immunogenicity of the HLA-A*02:01-restricted YLV-PIQFPV epitope, we extend these findings by successfully generating TCR-T cells with specificity for this epitope to develop alternative strategies to target this tumor antigen (43). Expanding on the work of Wei and colleagues (50) in which TCR-T cells were generated in a hepatocellular carcinoma model, we validated antigen-specific and TCR-T cell reactivity to this epitope in NSCLC and further identified TCRs recognizing FOXM1 in the context of HLA-A*02:01 and HLA-A*23:01. To the best of our knowledge, we are the first to generate FOXM1-specific TCR-T cells for HLA-A*02:01 and HLA-A*23:01. Additionally, our analysis of patient samples demonstrates that FOXM1-specific T-cell clonotypes are not exclusive to healthy individuals but are also present in patients with NSCLC, further demonstrating the feasibility and relevance of targeting FOXM1 in NSCLC.

We further established FOXM1 as a suitable target for cellular therapies, providing strong evidence of the cytotoxic potential of our TCR-T cells against FOXM1-expressing NSCLC cell lines. By leveraging the specificity and durability of TCR-T cell therapies, we present a promising approach to overcome FOXM1-driven NSCLC. FOXM1 expression did not seem confined to any particular genomic subtype of lung cancer, although alterations in RET, ALK, and FGFR1, among others, expressed increased levels of FOXM1. This could suggest FOXM1 is a promising target in these aggressive cancer subtypes with limited therapeutic options, although additional studies in larger patient cohorts are necessary. Specifically, this elevated FOXM1 expression observed in specific oncogenic subtypes, such as RET-driven tumors, suggests the possibility of prioritizing molecularly defined patient subsets. Moreover, as FOXM1 is induced in multiple cancer types (19, 51), our findings extend beyond NSCLC and highlight the potential for TCR-T cell therapies for the treatment of a variety of FOXM1-driven malignancies. The potential for on-target, off-tumor toxicity remains a critical consideration in the clinical translation of FOXM1-targeted TCR-T cell therapy. Although FOXM1 is minimally expressed in normal tissues, its transient expression in proliferating progenitor cells and during tissue regeneration highlight valid concerns about possible toxicity. Our data suggest the importance of thoroughly characterizing FOXM1 expression and TCR-T cell reactivity versus nonmalignant tissues as the lack of toxicity observed against healthy human brain, lung, liver, heart, and kidney cell lines is encouraging. Our analysis of TCR-T1 recognition by amino acid replacement provides further insight into the specificity of our TCR-T cells, highlighting the critical contacting residues for TCR-T cell recognition. We also demonstrate the endogenous expression of FOXM1 by tumors can be effectively targeted by TCR-T cells. Lastly, *in vivo* experiments demonstrated TCR-T cell persistence in addition to tumor reduction and prolonged survival, further highlighting the potential of this approach while exhibiting no signs of toxicity. This further emphasizes the safety and clinical applicability of FOXM1 TCR-T cells. Demonstrating the efficacy of this approach provides advancement in FOXM1-targeting therapeutics and also underscores the broader potential of TCR-T cell therapy in oncology. Overall, this study lays the foundation for clinical translation of these approaches to lung cancer and other solid tumors exhibiting high FOXM1 expression.

## Data Availability

TCR sequencing data are available at https://clients.adaptivebiotech.com/pub/reuben-2019-natcomms and https://clients.adaptivebiotech.com/pub/federico-2021-ao. Raw immunopeptidomics data are available through the Proteomics Identification Database under accession number PXD073612. Single-cell RNA-seq data of expanded FOXM1-specific TCR-T cells are available through the Gene Expression Omnibus under accession number GSE319956. Data are available to all researchers upon request.

## Authors' Disclosures

Y. Shulga reports grants from the NIH during the conduct of the study and personal fees from LASE Innovation, Inc. outside the submitted work and has financial interests in LASE Innovation, Inc. as an employee of the company. E. Paul reports grants from the American Lung Association during the conduct of the study. S. Forward reports grants from the NIH during the conduct of the study and personal fees from LASE Innovation, Inc. outside the submitted work and has financial interests in LASE Innovation, Inc. as an employee of the company. E.R. Assita reports grants from the NIH during the conduct of the study and personal fees from LASE Innovation, Inc. outside the submitted work and has financial interests in LASE Innovation, Inc. as an employee of the company. D. Deniger reports personal fees from Shennon Biotechnologies outside the submitted work. H.T. Tran reports personal fees from ABION BIO outside the submitted work. D.L. Gibbons reports grants and personal fees from Eli Lilly, personal fees from Aktis Oncology and Menarini Ricerche, and grants from Mirati/Bristol Myers Squibb, NGM Biopharmaceuticals, and Boehringer Ingelheim and outside the submitted work. I.I. Wistuba reports grants and personal fees from Roche/Genentech, Amgen, AstraZeneca, Merck, and Novartis, personal fees from Daiichi Sankyo, Boehringher Ingelheim, Merus, Guardant Health, Sanofi, AbbVie, Jansen, Regeneron, Johnson & Johnson, and Bristol Myeer Squibb, and grants from Takeda Bayer, Iovance, Karus, and EMD Serono outside the submitted work. J. Zhang reports grants and honoraria as a consultant, adviser, or speaker from AstraZeneca, BeiGene, Bicara, Bristol Myers Squibb, Catalyst, GenePlus, Henlius, Hengrui, Innovent Biologics, Johnson & Johnson, Merck, Novartis, OrigMed, Oncohost, Roche, Summit, Takeda, and Varian outside the submitted work. P. Hwu reports other support from Immatics, Dragonfly, and Adventris outside the submitted work. S. Kwok reports grants from the NIH during the conduct of the study and personal fees from LASE Innovation, Inc. outside the submitted work and has financial interests in LASE Innovation, Inc. as an employee of the company. A.M. Jaeger reports grants from the American Lung Association during the conduct of the study. J.V. Heymach reports a patent for "T-cell receptor recognizing an unmutated FOXM1 epitope presented on HLA-A*02:01" pending and a patent for "T-cell receptors targeting FOXM1 and methods of use thereof" pending. A. Reuben reports grants from Exon20 group, Rexanna's Foundation for Fighting Lung Cancer, Waun Ki Hong Lung Cancer Research Fund, MD Anderson's Lung Cancer Moon Shot, Salgado Family Charitable Fund, Troper Wojcicki Foundation, AACR Career Development Award in Lung Cancer Research, University Cancer Foundation via the Institutional Research Grant program at the University of Texas MD Anderson Cancer Center, Happy Lungs Project, EGFR Resisters, LUNGevity, RETpositive, CPRIT High Impact High Reward, CPRIT Individual Investigator Research Award, and SBIR Innovative Concept Award and other support from Tenaci-T Therapeutics LLC during the conduct of the study, as well as grants from Petrin Fund, NIH/NCI R21, DoD IDA, and CPRIT IIRA and other support from ATTACHbio LLC outside the submitted work; in addition, A. Reuben has a patent for "T-cell receptor recognizing an unmutated FOXM1 epitope presented on HLA-A*02:01" pending and a patent for "T-cell receptors targeting FOXM1 and methods of use thereof" pending. No disclosures were reported by the other authors.

## Authors' Contributions

**E. Bontekoe:** Conceptualization, data curation, formal analysis, investigation, visualization, writing–original draft, writing–review and editing. **M. Zhang:**

Conceptualization, data curation, formal analysis, validation, investigation, methodology, writing–review and editing. **P. Jiang:** Conceptualization, data curation, software, investigation, visualization, writing–review and editing. **A. Montoya:** Conceptualization, data curation, investigation, methodology, writing–review and editing. **Y. Shulga:** Data curation, investigation, writing–review and editing. **J.K. Slone:** Resources, data curation, software, investigation, visualization, writing–review and editing. **E. Paul:** Data curation, investigation, writing–review and editing. **C. Polera:** Data curation, investigation, writing–review and editing. **S. Forward:** Data curation, investigation, writing–review and editing. **B. Nassif Rausseo:** Data curation, investigation, writing–review and editing. **E.R. Assita:** Data curation, investigation, writing–review and editing. **C. Xing:** Methodology, writing–review and editing. **D.P. Molkentine:** Data curation, methodology, writing–review and editing. **B.B. Morris:** Writing–review and editing. **I. Polic:** Writing–review and editing. **J. Roszik:** Formal analysis, writing–review and editing. **R. Salgado:** Funding acquisition, writing–review and editing. **A. Vaishnavi:** Writing–review and editing. **D. Deniger:** Writing–review and editing. **H.T. Tran:** Resources, data curation, writing–review and editing. **D.L. Gibbons:** Resources, data curation, writing–review and editing. **A. Vaporciyan:** Writing–review and editing. **M.L. Gillison:** Writing–review and editing. **I.I. Wistuba:** Writing–review and editing. **L.E. Kavraki:** Writing–review and editing. **J. Zhang:** Resources, data curation, writing–review and editing. **G. Lizee:** Writing–review and editing. **C. Yee:** Resources, writing–review and editing. **P. Hwu:** Supervision, writing–review and editing. **S. Kwok:** Data curation, investigation, writing–review and editing. **A.M. Jaeger:** Conceptualization, data curation, formal analysis, investigation, writing–review and editing. **J.V. Heymach:** Supervision, writing–review and editing. **A. Reuben:** Conceptualization, resources, supervision, funding acquisition, writing–original draft, project administration, writing–review and editing.

## Acknowledgments

A. Reuben is supported by the Exon 20 Group, Rexanna's Foundation for Fighting Lung Cancer, the Lance Bertrand Research Grant, the Bruce Campbell Research Grant, the Waun Ki Hong Lung Cancer Research Fund, MD Anderson's Lung Cancer Moon Shot, the Petrin Fund, the Salgado Family Charitable Fund, the Troper Wojcicki Foundation, an NIH/NCI R21, a US Department of Defense Lung Cancer Research Program Idea Development Award, an AACR Career Development Award in Lung Cancer Research, the University Cancer Foundation via the Institutional Research Grant program at the University of Texas MD Anderson Cancer Center, the Happy Lungs Project, an EGFR Resisters/LUNGevity Foundation EGFR-positive research award, a RETpositive/LUNGevity Translational Research Award Program, a Cancer Prevention & Research Institute of Texas High Impact High Reward Award and a Cancer Prevention & Research Institute of Texas Individual Investigator Research Award for Computational Systems Biology of Cancer, a CPRIT Individual Investigator Research Award, and an SBIR NCI Innovative Concept Award. E. Bontekoe is supported by the T32 Translational Genomic and Precision Medicine in Cancer Predoctoral Fellowship. J.K. Slone is supported in part by the Big-Data Private-Cloud Research Cyberinfrastructure MRI-award funded by NSF under grant CNS-1338099 and by Rice University's Center for Research Computing (CRC). S. Kwok, Y. Shulga, S. Forward, E.R. Assita are supported in part by grants from the National Institutes of Health (R44CA281529). A. Vaishnavi is a CPRIT scholar in Cancer Research and is funded by CPRIT RR220062. The Advanced Cytometry & Sorting Core Facility is supported by NCI P30CA016672. The Advanced Technology Genomics Core was supported in part by The University of Texas MD Anderson Cancer Center, P30CA016672, and NIH 1S10OD024977-01. ICON was supported by the generous philanthropic contributions to The University of Texas MD Anderson Lung Cancer Moon Shots Program, the Gil and Dody Weaver Foundation and Bill and Katie Weaver Charitable Trust and the MD Anderson Cancer Center Support Grant P30 CA016672. A.M. Jaeger received funding from the American Lung Association Lung Cancer Discovery Award to support this work. Mass spectrometry was supported by the Proteomics and Metabolomics Shared Resource at Moffitt Cancer Center P30CA076292. J. Zhang reports research funding from Merck, Johnson and Johnson, Novartis, Summit, Hengenix and consultant fees from BMS, Johnson and Johnson, AstraZeneca, Geneplus, OrigMed, Innovent, Varian, Catalyst outside the submitted work. J.V. Heymach reports research funding from AstraZeneca, Boehringer-Ingelheim, Mirati, Bristol-Myer Squibb, Takeda, Taiho has served on advisory committees for AbbVie, Amgen, AnHeart Therapeutics, Arrivent, AstraZeneca, BioNTech AG, BI, BMS, Curio Science, DAVA Oncology, Eli Lily & Co, EMD Serono, Janssen Pharmaceuticals, Jazz Pharmaceuticals, Mirati Therapeutics, Moffitt Cancer Center, ModeX, Novartis Pharmaceuticals, OncoCyte, Pfizer, Sanofi, Spectrum Pharmaceuticals, Takeda, Ottimo Pharma, ALK Positive, served at speakers bureau for MJH Events, Guidepoint, Ideology Health and received licensing/royalties from Spectrum. D.L. Gibbons reports honoraria for scientific advisory boards from AstraZeneca, Sanofi, Alethia Biotherapeutics, Menarini Richerche, Eli Lilly, 4D Pharma, and Onconova and research support from Janssen, Takeda, Astellas, Ribon Therapeutics, Boehringer Ingelheim, NGM Biopharmaceuticals, Mirati Therapeutics, and AstraZeneca. P. Hwu serves as in the scientific advisory board for Dragonfly, Immatics, and Adventris. S. Kwok, Y. Shulga, S. Forward, E.R. Assita have financial interests in LASE Innovation Inc. A.M. Jaeger has received research support from RyboDyn Therapeutics. The intellectual property surrounding the TCRs included in this study is linked to WO2024123975A2.

## Note

Supplementary data for this article are available at Cancer Immunology Research Online (http://cancerimmunolres.aacrjournals.org/).

Received May 13, 2025; revised December 19, 2025; accepted March 17, 2026; posted first March 19, 2026.

## References

1. World Health Organization; [Lung cancer]. [cited 2025 Jan 6]. Available from: https://www.who.int/news-room/fact-sheets/detail/lung-cancer.
2. Molina JR, Yang P, Cassivi SD, Schild SE, Adjei AA. Non-small cell lung cancer: epidemiology, risk factors, treatment, and survivorship. Mayo Clin Proc 2008;83:584–94.
3. National Cancer Institue Surveillance, Epidemiology, and End Results Program. Cancer stat facts: lung and bronchus cancer. Bethesda (MD): National Cancer Institue; 2025.
4. World Health Organization; [Tobacco]. [cited 2025 Jan 6]. Available from: https://www.who.int/news-room/fact-sheets/detail/tobacco.
5. Alexander M, Kim SY, Cheng H. Update 2020: management of non-small cell lung cancer. Lung 2020;198:897–907.
6. Sharma P, Hu-Lieskovan S, Wargo JA, Ribas A. Primary, adaptive, and acquired resistance to cancer immunotherapy. Cell 2017;168:707–23.
7. Hiltbrunner S, Cords L, Kasser S, Freiberger SN, Kreutzer S, Toussaint NC, et al. Acquired resistance to anti-PD1 therapy in patients with NSCLC associates with immunosuppressive T cell phenotype. Nat Commun 2023;14:5154.
8. Zhou S, Yang H. Immunotherapy resistance in non-small-cell lung cancer: from mechanism to clinical strategies. Front Immunol 2023;14:1129465.
9. Brahmer JR, Lee JS, Ciuleanu TE, Bernabe Caro R, Nishio M, Urban L, et al. Five-year survival outcomes with nivolumab plus ipilimumab versus chemotherapy as first-line treatment for metastatic non-small-cell lung cancer in CheckMate 227. J Clin Oncol 2023;41:1200–12.
10. Mok T, Nakagawa K, Park K, Ohe Y, Girard N, Kim HR, et al. Nivolumab plus chemotherapy in epidermal growth factor receptor-mutated metastatic non-small-cell lung cancer after disease progression on epidermal growth factor receptor tyrosine kinase inhibitors: final results of CheckMate 722. J Clin Oncol 2024;42:1252–64.
11. Xie N, Shen G, Gao W, Huang Z, Huang C, Fu L. Neoantigens: promising targets for cancer therapy. Signal Transduct Target Ther 2023;8:9.
12. Lybaert L, Lefever S, Fant B, Smits E, De Geest B, Breckpot K, et al. Challenges in neoantigen-directed therapeutics. Cancer Cell 2023;41:15–40.
13. Leko V, Rosenberg SA. Identifying and targeting human tumor antigens for T cell-based immunotherapy of solid tumors. Cancer Cell 2020;38:454–72.
14. Pearlman AH, Hwang MS, Konig MF, Hsiue EH, Douglass J, DiNapoli SR, et al. Targeting public neoantigens for cancer immunotherapy. Nat Cancer 2021;2:487–97.
15. Chen X, Müller GA, Quaas M, Fischer M, Han N, Stutchbury B, et al. The forkhead transcription factor FOXM1 controls cell cycle-dependent gene expression through an atypical chromatin binding mechanism. Mol Cell Biol 2013;33:227–36.

16. Myatt SS, Lam EW. The emerging roles of forkhead box (Fox) proteins in cancer. Nat Rev Cancer 2007;7:847–59.
17. Kong FF, Qu ZQ, Yuan HH, Wang JY, Zhao M, Guo YH, et al. Overexpression of FOXM1 is associated with EMT and is a predictor of poor prognosis in non-small cell lung cancer. Oncol Rep 2014;31:2660–8.
18. Nilsson MB, Sun H, Robichaux J, Pfeifer M, McDermott U, Travers J, et al. A YAP/FOXM1 axis mediates EMT-associated EGFR inhibitor resistance and increased expression of spindle assembly checkpoint components. Sci Transl Med 2020;12:eaaz4589.
19. Liao GB, Li XZ, Zeng S, Liu C, Yang SM, Yang L, et al. Regulation of the master regulator FOXM1 in cancer. Cell Commun Signal 2018;16:57.
20. Rodríguez-Cruz TG, Liu S, Khalili JS, Whittington M, Zhang M, Overwijk W, et al. Natural splice variant of MHC class I cytoplasmic tail enhances dendritic cell-induced $CD8^+$ T-cell responses and boosts anti-tumor immunity. PLoS One 2011;6:e22939.
21. The Cancer Genome Atlas (TCGA). [cited 2025 Jan 3]. Available from: https://www.cancer.gov/ccg/research/genome-sequencing/tcga
22. The GTEx Portal. GTEx Consortium [cited 2025 Jan 3]. https://www.gtexportal.org/home/.
23. Reuben A, Zhang J, Chiou SH, Gittelman RM, Li J, Lee WC, et al. Comprehensive T cell repertoire characterization of non-small cell lung cancer. Nat Commun 2020;11:603.
24. Schmidt ST, Akhave N, Knightly RE, Reuben A, Vokes N, Zhang J, et al. Shared nearest neighbors approach and interactive browser for network analysis of a comprehensive non-small-cell lung cancer data set. JCO Clin Cancer Inform 2022;6:e2200040.
25. Reynisson B, Alvarez B, Paul S, Peters B, Nielsen M. NetMHCpan4.1 - DTU Health Tech - Bioinformatic Services; 2020. [cited 2025 Jan 3]. Available from: https://services.healthtech.dtu.dk/services/NetMHCpan-4.1/.
26. Kraemer AI, Chong C, Huber F, Pak H, Stevenson BJ, Müller M, et al. The immunopeptidome landscape associated with T cell infiltration, inflammation and immune editing in lung cancer. Nat Cancer 2023;4:608–28.
27. Rosenberg SA, Dudley ME. Adoptive cell therapy for the treatment of patients with metastatic melanoma. Curr Opin Immunol 2009;21:233–40.
28. Karimi MA, Lee E, Bachmann MH, Salicioni AM, Behrens EM, Kambayashi T, et al. Measuring cytotoxicity by bioluminescence imaging outperforms the standard chromium-51 release assay. PLoS One 2014;9:e89357.
29. Hughes MS, Yu YY, Dudley ME, Zheng Z, Robbins PF, Li Y, et al. Transfer of a TCR gene derived from a patient with a marked antitumor response conveys highly active T-cell effector functions. Hum Gene Ther 2005;16:457–72.
30. Yang S, Cohen CJ, Peng PD, Zhao Y, Cassard L, Yu Z, et al. Development of optimal bicistronic lentiviral vectors facilitates high-level TCR gene expression and robust tumor cell recognition. Gene Ther 2008;15:1411–23.
31. Rasko JE, Battini JL, Gottschalk RJ, Mazo I, Miller AD. The RD114/simian type D retrovirus receptor is a neutral amino acid transporter. Proc Natl Acad Sci U S A 1999;96:2129–34.
32. Zhang M, Fritsche J, Roszik J, Williams LJ, Peng X, Chiu Y, et al. RNA editing derived epitopes function as cancer antigens to elicit immune responses. Nat Commun 2018;9:3919.
33. Kwok SJJ, Forward S, Fahlberg MD, Assita ER, Cosgriff S, Lee SH, et al. High-dimensional multi-pass flow cytometry via spectrally encoded cellular barcoding. Nat Biomed Eng 2024;8:310–24.
34. Yamamoto T, Price DA, Casazza JP, Ferrari G, Nason M, Chattopadhyay PK, et al. Surface expression patterns of negative regulatory molecules identify determinants of virus-specific $CD8^+$ T-cell exhaustion in HIV infection. Blood 2011;117:4805–15.
35. Altosole T, Rotta G, Uras CRM, Bornheimer SJ, Fenoglio D. An optimized flow cytometry protocol for simultaneous detection of T cell activation induced markers and intracellular cytokines: application to SARS-CoV-2 immune individuals. J Immunol Methods 2023;515:113443.
36. Meddows-Taylor S, Shalekoff S, Kuhn L, Gray GE, Tiemessen CT. Development of a whole blood intracellular cytokine staining assay for mapping CD4(+) and CD8(+) T-cell responses across the HIV-1 genome. J Virol Methods 2007;144:115–21.
37. Yin R, Ribeiro-Filho HV, Lin V, Gowthaman R, Cheung M, Pierce BG. TCRmodel2: high-resolution modeling of T cell receptor recognition using deep learning. Nucleic Acids Res 2023;51:W569–76.
38. Jumper J, Evans R, Pritzel A, Green T, Figurnov M, Ronneberger O, et al. Highly accurate protein structure prediction with AlphaFold. Nature 2021;596:583–9.
39. Gowthaman R, Pierce BG. TCR3d: the T cell receptor structural repertoire database. Bioinformatics 2019;35:5323–5.
40. Chandran SS, Ma J, Klatt MG, Dündar F, Bandlamudi C, Razavi P, et al. Immunogenicity and therapeutic targeting of a public neoantigen derived from mutated PIK3CA. Nat Med 2022;28:946–57.
41. Bradley SD, Talukder AH, Lai I, Davis R, Alvarez H, Tiriac H, et al. Vestigial-like 1 is a shared targetable cancer-placenta antigen expressed by pancreatic and basal-like breast cancers. Nat Commun 2020;11:5332.
42. Okuno K, Sugiura F, Inoue K, Sukegawa Y. Clinical trial of a 7-peptide cocktail vaccine with oral chemotherapy for patients with metastatic colorectal cancer. Anticancer Res 2014;34:3045–52.
43. Yokomine K, Senju S, Nakatsura T, Irie A, Hayashida Y, Ikuta Y, et al. The forkhead box M1 transcription factor as a candidate of target for anti-cancer immunotherapy. Int J Cancer 2010;126:2153–63.
44. Liu W, Tang H, Li L, Wang X, Yu Z, Li J. Peptide-based therapeutic cancer vaccine: current trends in clinical application. Cell Prolif 2021;54:e13025.
45. Hasegawa K, Ikeda Y, Kunugi Y, Kurosaki A, Imai Y, Kohyama S, et al. Phase I study of multiple epitope peptide vaccination in patients with recurrent or persistent cervical cancer. J Immunother 2018;41:201–7.
46. Garg P, Pareek S, Kulkarni P, Horne D, Salgia R, Singhal SS. Next-generation immunotherapy: advancing clinical applications in cancer treatment. J Clin Med 2024;13:6537.
47. Raghuwanshi S, Zhang X, Arbieva Z, Khan I, Mohammed H, Wang Z, et al. Novel FOXM1 inhibitor STL001 sensitizes human cancers to a broad-spectrum of cancer therapies. Cell Death Discov 2024;10:211.
48. Zhang Z, Xue ST, Gao Y, Li Y, Zhou Z, Wang J, et al. Small molecule targeting FOXM1 DNA binding domain exhibits anti-tumor activity in ovarian cancer. Cell Death Discov 2022;8:280.
49. Raghuwanshi S, Gartel AL. Small-molecule inhibitors targeting FOXM1: current challenges and future perspectives in cancer treatments. Biochim Biophys Acta Rev Cancer 2023;1878:189015.
50. Wei T, Zeng C, Li Q, Xiao Z, Zhang L, Zhang Q, et al. FOXM1/DEPDC1 feedback loop promotes hepatocarcinogenesis and represents promising targets for cancer therapy. Cancer Sci 2024;115:3041–53.
51. Pozzobon D, Bellezza A, Giorgi FM. Pan-cancer upregulation of the FOXM1 transcription factor. Genes (Basel) 2025;16:56.